Towards milli-Kelvin Scanning Tunneling Microscopy with atomic resolution

van der Ven, João

Towards milli-Kelvin Scanning Tunneling Microscopy with atomic resolution

THESIS

submitted in partial fulfillment of the
requirements for the degree of

MASTER OF SCIENCE
in
PHYSICS

Author :	João-Maurits Marie van der Ven
Student ID :	2057263
Supervisor :	Prof.dr.ir. T.H. Oosterkamp
	K. van Deelen (PhD)
Second corrector :	Prof. dr. J.M. van Ruitenbeek

Leiden, The Netherlands, March 7, 2024

Towards milli-Kelvin Scanning Tunneling Microscopy with atomic resolution

João-Maurits Marie van der Ven

Huygens-Kamerlingh Onnes Laboratory, Leiden University
P.O. Box 9500, 2300 RA Leiden, The Netherlands

March 7, 2024

Abstract

This research aims to develop a Scanning Tunneling Microscope (STM) at milli-Kelvin temperatures inside a dry-dilution refrigerator, at the *Oosterkamp Group*. Getting the STM to operate properly in these extreme conditions will allow us to do scanning and spectroscopy measurements with improved resolution. However, these extreme conditions also give rise to challenges. Specifically, we analyse the contributions of the pulse tube, which causes mechanical and acoustical vibrations. We determined that the dominant vibrations entered through microphonics around the I/V-converter and its cables. This gave rise to 30 pA_{RMS} noise. By mounting the I/V-converter directly to the cryostat and fixing the cables we successfully reduced the effect of microphonics to an upper-bound of 4 pA_{RMS}, and see potential to improve on this result. Through the feedback system this upper-bound would give rise to 0.02 Å RMS amplitude oscillations of the tip-sample distance. This should not prevent us from achieving step-edge resolution or atomic resolution. Furthermore, we present new scans at room-temperature with significantly improved resolution and a scan at ultra-low temperature with a visible step-edge for the first time since 2014.

Contents

Version of March 7, 2024– Created March 7, 2024 - 11:58

Chapter 1

Introduction

We humans want to understand the world we live in, and science is a way to make progress. It is based on doing observations, analysis and drawing conclusions, to understand and predict the future. To do observations we need to be able to look. To the largest objects around us like stars and black holes but also the smallest objects like atoms and electrons. We need 'eyes'. In the 16th century the first telescope was build in the Netherlands, an apparatus to look at the largest structures in the cosmos and allowed us to observe radiation dating back to the very beginning of our universe. Three centuries later, in 1981, G. Binning and H. Rohrer [3], invented the *Scanning Tunneling Microscope (STM)*, a 'telescope' to observe the smaller particles in our universe. An instrument that is able to observe samples with *atomic resolution*, i.e. the ability to distinguish individual atoms. Decades later this technology has produced us many images with atomic resolution [12, 20, 1, 18, 2], allowing us to study the realm of the smallest.

While the physical principles behind the STM are relatively straightforward, the conditions at which we, at the *Oosterkamp Group*, try to achieve atomic resolution are highly challenging. Namely, by placing our STMs inside a dry dilution refrigerator, striving to operate in extreme conditions with ultra-low temperatures, ultra-high vacuum and high acoustical-, mechanical- and electromagnetic isolation. These conditions would lead us to scans with higher spatial resolution and spectroscopy with higher energy resolution. Allowing us to better explore the properties of materials, ultimately using them to our advantage. At the *Oosterkamp Group* atomic resolution scans inside a dry-dilution refrigerator have been achieved by den Haan et al. (2014)[12]. However, progress laid still for a couple of years and the ability to produce a scan with atomic resolution, as well as some of the experience, was lost. Until K. van Deelen started his PhD on

developing STMs again. The most recent STM makes use of new cryo-walking technology to approach the tip to the sample. The cryo-walker operates in the lowest loss factor regime of the piezo material, resulting in the lowest heat dissipation [27]. Walking and approaching with these new motors was successful, although not yet consistent enough. Scans at room temperature seem to indicate height differences, but the resolution is not good enough to observe clear step-edges, let alone atomic resolution. Scans done with the STMs inside an operating dry dilution refrigerator show no signs of atomic features up to now. One of the challenges of achieving a high resolution is reducing all the sources of noise and interference. To this matter, the dry dilution refrigerator has many benefits, but it also causes mechanical and acoustical vibrations due to the so called *pulse tube*, that is needed for the cooling mechanism. At this point the severity of the vibrating pulse tube is unknown. Will it prevent us from achieving atomic resolution? And how do we reduce its contribution?

This research is about developing and implementing the *Basic-STM* at the *Oosterkamp Group*, such that it can consistently approach and do measurements with improved resolution at milli-Kelvin temperatures inside a dry dilution refrigerator. Furthermore, we want to understand the different noise sources and reduce their contributions as much as possible. To this end, we have analyzed one of the contributors to the mechanical noise, the pulse tube, which pumps at 1.4Hz. Finally, we analyse scanning measurements with improved resolution.

In chapter 2 we lay down the theoretical background and other important aspects. We will describe the physical principle behind the STM, what kind of measurements we can do with it and what are the challenges for achieving a high resolution. Furthermore, we explain what a cryostat is and describe the unique aspects of the cryostat that houses our STMs. In chapter 3 we explain the methodology and implementation. We will explain how we produced tips and samples and how we were able to approach the tip delicately to the sample, without crashing. Furthermore, we map out the different noise sources we are facing and explain how we are going to analyse the contributions of the pulse tube. In chapter 4 we present the experiments that we have conducted in order to explore the contribution from the pulse tube, discuss our findings and explain how we succeeded to reduce the effect of microphonics. Lastly, we present scanning results. In chapter 5 we draw our conclusion and give an outlook.

Chapter 2

Theory

In this chapter we cover the theoretical background upon which this research is based on. We start by describing the physical principles behind an STM and the electrical components that compose it. Furthermore, we explain the types of measurements an STM allows us to conduct, why they are relevant and why they are challenging. Finally, we close the chapter by explaining the unique properties of the *Marshmallow* cryostat, the dry-dilution refrigerator that houses our STMs.

2.1 Scanning Tunneling Microscope (STM)

The STM relies on a quantum mechanical phenomenon called *quantum tunneling*. The effect that a charged particle can overcome - and 'tunnel' through - a potential barrier while, if viewed classically, it does not have enough energy to overcome that barrier [21]. By bringing a conducting tip close enough to a conducting sample and applying a bias voltage V_b, such that the wave-form of the particle crosses the gap, a *tunnel-current* will start to flow [28]. Now, the magnitude of this current $I(z)$ depends exponentially on the distance between the two objects z through [7]:

$$I(z) = I(0)e^{-2\kappa z} \tag{2.1}$$

where, $\kappa = \sqrt{2m\Phi}/\hbar$, is the decay constant, m is the mass of the charge carrier and $\hbar$ is the reduced Planck's constant. The Fermi work function, $\Phi = V_0 - E_F$ [30], describes the minimum energy that is required to remove an electron from the Fermi level of the metal E_F to the vacuum level V_0 [7]. $I(0)$ is the impinging current at $z = 0$ [7], determined by the bias

voltage V_b we apply to the sample. A graphical representation of the exponential decay through a 1D vacuum barrier is presented in fig. 2.1. Since the tunnel-current depends on the distance between the tip and the sample z, we can use its magnitude as a measure for the distance, when keeping the bias voltage constant. Additionally, we can change the bias voltage while keeping the distance constant and observer how this influences the tip-current. Next to the distance dependency, the tunnel-current also depends on what is called the density of states (DOS), which has profound implications that we will discuss in sec. 2.2. Ultimately these properties and principles give rise to two types of measurements called *scanning* and *spectroscopy*, which we will explain more thoroughly in sec. 2.2. The basic schematics of the STM are shown in fig. 2.2.

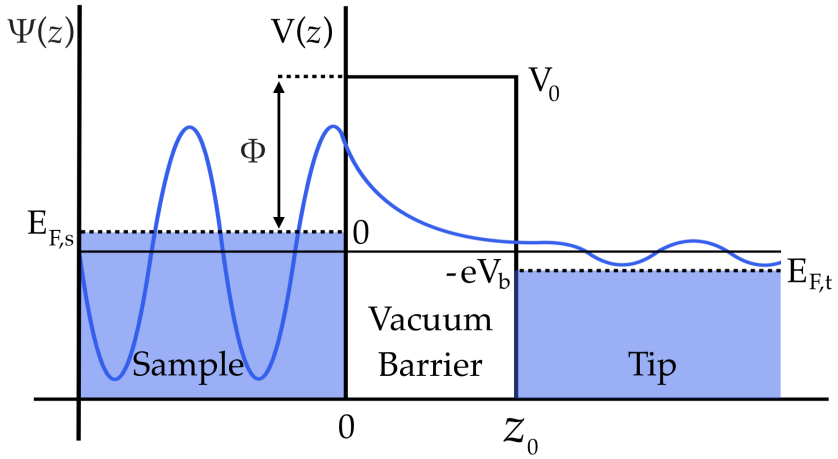

Figure 2.1: *Representation of the exponential decay of the wave function $\Psi(z)$ through a 1D vacuum barrier extending from $z = 0$ to $z = z_0$. Inspired on a figure from F. Trixler (2019) [30]. Φ denotes the local Fermi work function, i.e. the minimum energy required to remove an electron from the metal to the vacuum level V_0 [30]. With a bias voltage V_b applied on the sample causing the Fermi level of the sample $E_{F,s}$ to shift with respect to the Fermi level of the tip $E_{F,t}$. Blue denotes occupied states.*

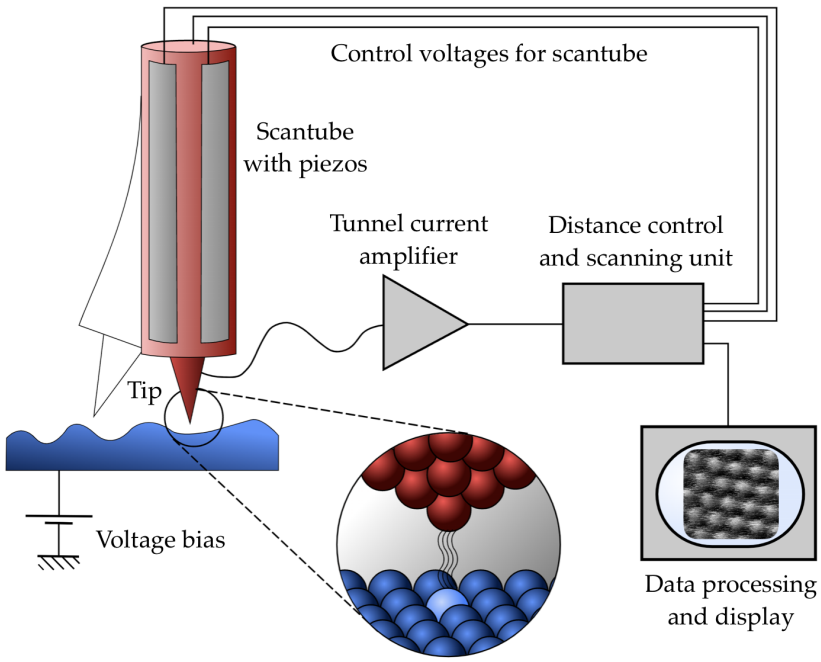

Figure 2.2: *Schematics of a Scanning Tunneling Microscope (STM) from: [25]. The tunnel-current is amplified by the 'Tunnel current amplifier' or 'I/V-converter' and sent tho the PI-feedback controller in order to control the voltages on the scan tube. The scan (Data processing and display) is from den Haan et al. [12], in which the atomic structure of graphene is visible, at 15mK.*

Tip and sample

The *tip* must have a couple of properties. First of all, since the principle behind the STM is quantum tunneling of electrons, we need a material that contains free-electrons. Hence, tips are made from metals. Furthermore, it is desired that the Local Density of States (LDOS), a physical property of a material that will be explained in section 2.2, is as flat as possible, because this way we can separate the properties from the sample from those of the tip. Finally, in order to achieve atomic resolution, the tip needs to be atomically sharp. Preferably a single atom thick, however, this is hard to achieve [5]. Generally, the apex of the tip is of the order of tens of nanometers. Which means that the tip is many atoms wide. However, some atoms will be sticking out more than others, which become the dominating contribution to the current. If multiple equally sticking-out-atoms are close to each other, 1 nm for instance, the current will equally flow along both paths, effectively causing a feature to be measured twice, we call this a *double-tip*, which is undesired as it spreads the spatial resolution. In the

appendix we present an example of a scan where we observed the effect of a double-tip (fig. 4.13). Mainly there are two methods for producing sharp tips: cutting and etching. The *cutting* method uses basic scissors at a 45 degrees angle cut while having simultaneous tension on both sides of the wire [22]. The second method, and the method that we implemented for our research is that of *electrochemical etching*. The wire is placed inside a conducting ring containing a meniscus of basic solution. Then, by applying a voltage across the wire and the ring, chemical etching occurs at the wire, close to the ring, making it locally thinner. [22]. In section 3.1 we explain our implementation of etching the STM-tips.

To characterize and calibrate our STM we especially desire a well known *sample*, that is also easy to replace. Furthermore, it is desired that it contains flat surfaces of conductive crystal, called *terraces*. Because, if the surface contains very steep edges and height differences, the feedback will have a harder time at keeping a constant current. Usually, a sample contains multiple terraces of different heights. At some point a new terrace is formed on top of an existing layer. Typically, the two layers differ in height by a single atom. In section 3.1 we explain why we used Highly Oriented Pyrolytic Graphite (HOPG) as our sample and how we prepared it.

Piezo elements and scan tube

In order to manoeuvre the tip and sample with high precision at the atomic scale, i.e. Ångström distances, we make use of *piezoelectric actuators*. Who's functioning relies on the *piezoelectric effect*, discovered in 1880 by two French brothers, Jacques and Pierre Curie [10], where applying pressure to certain crystals result in an electric charge. Later they also discovered the *inverse* piezoelectric effect, where applying an electrical field results in the generation of mechanical strain. For these materials there are regimes of applied electrical field that cause linear but most importantly predictable mechanical strain. Which makes it consistent, precise and functional. The total strain depends on the total capacitance of the piezo which typically reduces 4 or 5 times in the ultra cold conditions of the cryostat. This is relevant because there is a maximum voltage that we can apply to each piezo, which makes it extra challenging to operate these piezo motors at ultra low temperatures.

In an STM, piezos are used in two types of components: the *motors* and the *scan tube*. The motors are used to approach the tip to the desired location of the sample. This is a very delicate process as the tip may not crash into the sample. In section 3.2 we discuss how we succeeded in doing this.

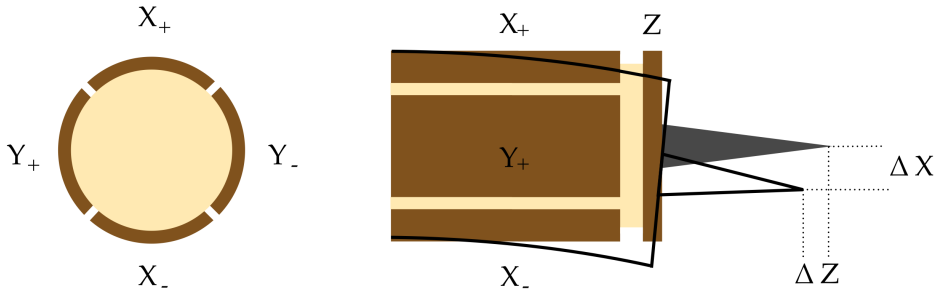

Figure 2.3: *The electrodes layout of the scan tube. Left: cross section. Right: sideview. Brown parts are the electrodes that are connected to the piezo crystal denoted in beige. Right: Example of a tilt in the X-direction of the scan tube. In this case we've applied a voltage across X_+, X_-, causing a tilt in the X-direction. Notice that this also caused a shift in the Z-coordinate of the tip. Thus, if we want to stay at the same Z-coordinate the Z-piezo needs to extend as well.*

Once close enough, the scan tube is used to bring the tip into tunneling-range and scan a sample. The scan tube is a piezo crystal that contains 5 electrodes, X_+, X_-, Y_+, Y_- to tilt the tip into the X and Y directions and Z to extend or retract the tip. The piezo-layout is shown in figure 2.3. Furthermore, an example of a tilt into the X-direction is also shown in figure 2.3. Different than you might initially expect, to do a scan all 5 piezos are being used at the same time. Because when we tilt the tip into some X,Y-direction, the Z-coordinate of the tip will automatically decrease (see figure 2.3), to accommodate for this the Z-piezo needs to extend as well.

Lock-in amplifier, I/V-converter and low-pass filter

In the previous sections we described the fundamental constituents of the STM. Here, we describe our measurement devices, such as a lock-in amplifier, an I/V-converter and a low-pass filter. This section explains why we use these in our setup.

In many cases when working on the setup or doing measurement we are working with oscillating signals, but also with noisy signals. A *lock-in amplifier* is extremely good at extracting the amplitude of a periodic signal at a certain frequency. One of the first instances where we make use of the lock-in amplifier is when we are approaching the tip to the sample. As explained in section 3.2, the amplitude at a specific frequency is what determines the capacitance read-out of the STM-junction, which allows us to observe if the tip is indeed moving towards the sample. Moreover, as we will cover in section 2.2, we can use the lock-in amplifier to do spec-

troscopy and produce dI/dV-curves.

The *I/V-converter* (or "Tunnel current amplifier" in figure 2.2), is used to convert and amplify the tunneling current into a measurable voltage. Because a voltage is more easy to record and can be connected to several measurement devices without interfering with the signal. Such an I/V-converter also has a specific gain G. In our case, we can expect a tip-current of the order ~ 1 nA, and we set the gain G to 10^9, such that we convert the tip-current to $1V$ voltage. We want to amplify it because measuring, with precision, a signal of the order of $\sim$ 1nA would be challenging. For this research we used the *Femto DLCPA-200* current amplifier, which contributes a noise floor that we cover in section 3.3.

Finally, we also connect a *low-pass filter* to the tip-current cable before recording it with the DAQ (Digital to Analog converter). Our signal contains noise throughout the entire frequency range (white noise for instance). If we are going to measure our signal using a certain sampling frequency, all the noise of the higher frequencies will still enter and show up incorrectly at low frequencies [14], making troubleshooting and hunting down noise and interference difficult. Therefore, we are looking for a component that is able to cut-off signals above a certain frequency f_c, i.e. a low-pass filter. We attached a second order RC low-pass filter with cutoff-frequency $f_c = 200Hz$. Second order meaning that the filter has a -40 dB/dec decay of the signal after the cut-off frequency.

2.2 Scanning and Spectroscopy

Now that we have explained the principle components of an STM, we will proceed with explaining what types of measurements we can do with it, how do we produce such measurements and what are challenges and limiting factors to consider. Generally, we use the STM for two types of measurements: *scanning* and *spectroscopy*. Where scanning is done over an entire area of the sample, spectroscopy is done at a specific location. Both having their one set of challenges.

Scanning

First of all, we can *scan* the sample, meaning that we move the tip in a grid across the sample, either in a constant height mode, or in a constant current mode. In *constant height mode* we keep the tip at a constant height (Z), in tunneling range, while moving past the atoms (X,Y). The topography and LDOS will change and with that the current we measure as well. In

constant current mode, while moving past the atomic structure, we change the height of the tip (using the Z-piezo on the scan tube, sec. 2.1), in order to maintain a constant current. The change in height is automated by a PI-feedback system. If the measured current exceeds the desired set-point value, the voltage to the scan tube is lowered such that the tip-sample distance increases, which decreases the tunnel current. The proportional (P) feedback is proportional to the error between the current value and the set-point, while the integral (I) feedback provides an integration of the past values as well, and can average out parts of the deviations. The PI-feedback is either analogically determined in the *LPM-rack*, a control component developed by *Leiden Probe Miscroscopy (LPM)*. Or digitally using *Nanonis*, which nowadays is fast enough and in our experience more convenient. If feedback is able to completely stabilize the current at a constant value, then all the topographical information is given by the feedback signal, as we can relate this to a change in height. While the *constant height mode* is generally faster, it is harder to extract the precise topographic features of a sample. Also, the risk of crashing the tip is higher as it will not retract the tip when it moves too close to the sample. Furthermore, *piezo-creep* can be a problem, the effect where the crystal continues to expand after we stop to apply a voltage. The main disadvantage of the constant current mode is that the integration time of the PI-feedback slows done the scanning.

What is interesting, is that we are not actually measuring the physical topography. We are measuring something that is closely related to the physical topography, and therefore 'interpret' a scan as the topography, while we are in fact measuring the amount of electrons that could possibly tunnel at each specific location. If this amount would only depend on the height, our measurement would be a direct measurement of the physical topography. However, apart from the geometry, the current also depends on what is called the *Density of States (DOS)* [28], the amount of different states, at a specific energy level, that are available for electrons to occupy. This DOS varies from point to point and from energy level to energy level, called the *Local Density Of States (LDOS)*. It is one of the most useful quantities for understanding and fundamentally describing the conductive properties of materials. For instance properties that have an electric or optical origin can be deduced from the DOS [29].

Generally, the units for x and y in scans are expressed in nanometers (10^{-9} m), while z is expressed in picometers (10^{-12} m) [7]. Obtaining a scan with atomic resolution has successfully been done in the *Oosterkamp Group* by den Haan et al. in 2014 [12] (figure 2.7), in a different cryostat, but never since. Progress laid still for a couple of years and the ability to

produce a scan with atomic resolution inside a dry dilution refrigerator, as well as some of the experience, was lost. Until K. van Deelen started his PhD on STM in the *Oosterkamp Group*. Only at room temperature, a scan that seems to indicate height-differences has been achieved by K. van Deelen and M. Stallen in 2023 (fig. 2.6), but the resolution is not good enough to observe clear step-edges, let alone atomic resolution. Achieving a scan with improved resolution or possibly with atomic resolution, at ultra-low temperatures is one of the aims of this research.

Resolution of scanning

A sample has different types of features. Bigger features that are easier to distinguish, and smaller features, that require a better resolution. The largest and therefore easiest feature that we could measure is a *step-edge*, the transition where one terrace lays on another one. This is a feature that is conveniently apparent when scanning a surface of several hundreds of nanometers (see figures 2.6 and 4.12). The great size of the surface and a relatively fast scan speed (one line/s = thousands of atoms/s), with respect to a scan aiming to distinguish individual atoms, means that the integration time of the integral feedback covers many more atoms, averaging out part of the features and the noise. Typically, the two layers differ in height by a single or sometimes multiple atoms. As will be explained later in section 3.1, we used HOPG, for which the distance between two single layers is about 3.35Å. Hence, a step-edge will always be a multiple of 3.35Å. If we want our STM to distinguish individual step-edges, we need a resolution sufficiently below 3.35 Å. There is no exact rule as to what resolution one needs in order to be able to distinguish features that are a certain distance apart, but our first assumption is that we need a resolution at least half of the feature we are trying to observe. Which means that the amplitude of our uncertainty may not exceed 1.7 Å, as visualised in figure 2.4, for *constant height mode*.

But, what does this mean for the measured current while moving past step-edges that separate terraces of different heights, when scanning in *constant height mode*. And what does this mean for the allowed current-noise? Relation 2.1 relates the tunnel-current and tip-sample distance and describes the exponential decay of current with increasing distance. Which implies that for every 1 Å increase in distance, the current increases roughly 10 times. Let's try to get a feeling for the amount of noise we are allowed to have, in order to still obtain a certain resolution for a certain set-point I_{sp} and bias voltage V_b. From equation 2.1 we know that the measured tip-current around a set-point $I_{sp}(z_0)$ would cause the tip-sample distance

to be z_0 according to:

$$\frac{I_{sp}(z_0)}{I(0)} = e^{-2\kappa z_0} \tag{2.2}$$

Where, $\kappa = 5.123\sqrt{\phi(eV)}/nm^{-1}$. C.J. Chen [7] lists the typical values of work functions ϕ and corresponding decay constants κ, also including Tungsten (W), in Table 1.1. Typical value for κ are all around $\kappa = 10nm^{-1}$, so we take this value here as well. Furthermore, we know if the tip-sample distance decreases with Δz, the measured tip-current $I(z_0 - \Delta z)$ will increase and be related through:

$$\frac{I(z_0 - \Delta z)}{I(0)} = e^{-2\kappa(z_0 - \Delta z)} \tag{2.3}$$

Now, we can find the relation between the measured tip-current around a set-point $I_{sp}(z_0)$ and the measured tip-current $I(z_0 - \Delta z)$ if the tip-sample distance has been increased by Δz, by dividing equations 2.2 and 2.3, such that we obtain:

$$\frac{I(z_0 - \Delta z)}{I_{sp}(z_0)} = \frac{e^{-2\kappa(z_0 - \Delta z)}}{e^{-2\kappa z_0}} \tag{2.4}$$

Which reduces to the following relation:

$$\frac{I(z_0 - \Delta z)}{I_{sp}(z_0)} = e^{2\kappa \Delta z} \tag{2.5}$$

Using relation 2.5, we can determine the order of the currents in *constant height mode*, while moving past step-edges separating terraces of different heights, and assuming a noise not more than half the feature we are trying to distinguish. The resulting currents are shown in figure 2.4. For instance, substituting $I_{sp} = 100pA$, $\kappa = 10\text{nm}^{-1}$ and $\Delta z = 0.17$nm, the right hand side of equation 2.5 reduces to $e^{2 \cdot 10 \cdot 0.17} \sim 30$. Meaning that the resulting current when observing a feature 1.7 Å closer, would be $30 * I_{sp} = 3$ nA. Likewise, if due to vibrations the tip moves 1.7 Å closer, the measured current will be 3 nA. On the other hand, a feature 1.7 Å farther would result in a current $e^{2 \cdot 10 \cdot -0.17} \sim 0.03$ times smaller, i.e. 3 pA. When the tip crosses a step-edge seperating two layers of graphene, the atoms in the next layer produce a current of 100 fA, and if due to vibrations the tip-sample distance increases by 1.7Å, we reach 4 fA, which is already drowned by the noise floor of the I/V-converter (sec. 3.3). This problem does not arise when measuring in *constant current mode*, which has the benefit that we

ensure measuring the tip-current in a regime that we desire. This way, we do not have to worry that our signal is drowned by other noise floors.

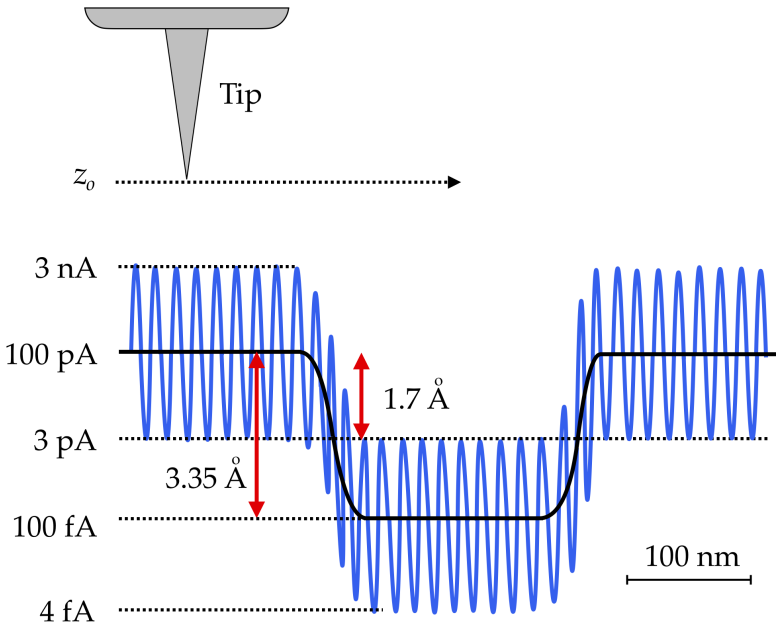

Figure 2.4: *Schematic representation of the current when scanning in constant height mode across step-edges. Black: pure contribution of HOPG layers. Blue: measured data including the noise. In this case the amplitude of the noise, 1.7 Å, is half of the feature we are trying to distinguish, the distance between two layers of HOPG* 3.35Å*. This ensures that we are able to distinguish the feature. Furthermore, it shows how a change of height at the order of HOPG features influences the measured current.*

The next goal would be the ability to distinguish the individual carbon atoms. One could think that this again only requires us to be able to distinguish the distance between an atom and the underlying layer of HOPG. Unfortunately, it is not as straightforward as that. The measured current is the sum of the contributions of all the neighbouring atoms. And because the current decays exponentially with distance, the configuration and contribution of the nearest neighbours, next-nearest neighbours, next-next-nearest neighbours, and so on, differs at each tip-location. We have visualised this concept in fig. 2.5, which is a 1D simplified model, because in reality atoms in consecutive layers are not in the same plane. Now, atomic resolution, i.e. the ability to distinguish individual atoms actually implies being able to distinguish the magnitude of the current directly above an atom, to that of the current when hovering between atoms. Which are both of higher magnitude then when measuring exclusively atoms in the 2nd layer. This difference reveals why one needs a better resolution to distinguish individual atoms, compared to distinguishing layers of HOPG. For future research it would be interesting to quantify this difference in needed resolution by simulating the positions of the atoms and the resulting contribution to the measured current using the characteristic lengths of HOPG and the hexagonal and three dimensional geometry. Probably limiting ourselves to the nearest and next-nearest atoms to prevent a too complex or time-consuming calculation. Furthermore, striving for atomic resolution gives rise to another challenge related to the integral component of the PI-feedback. In order for the integral component not to average-out contributions of individual atoms, the integration time may not be larger than the time it takes for the scan tube to pass an atom. For instance, if we make a 2.14 nm $\times$ 2.14 nm scan (fig. 2.7), containing roughly 9×9 atoms, and we scan with 1 line/s, this implies that the scan tube takes about $1/9 = 0.11$ seconds per atom. This puts a limit at 0.11 seconds to our integration time, which means that we are very sensitive to noise up to $1/0.11 = 9$Hz. Pointing to the need to suppress low frequency mechanical and acoustic noise, like the 1.4 Hz noise caused by the pulse tube.

A finer feature, that requires an even higher resolution, would be one that many atoms collectively form, like the "herringbone" reconstruction of gold for instance. Where every atom is positioned only slightly higher or lower to its neighbour and together, on a greater scale, forms a finer structure.

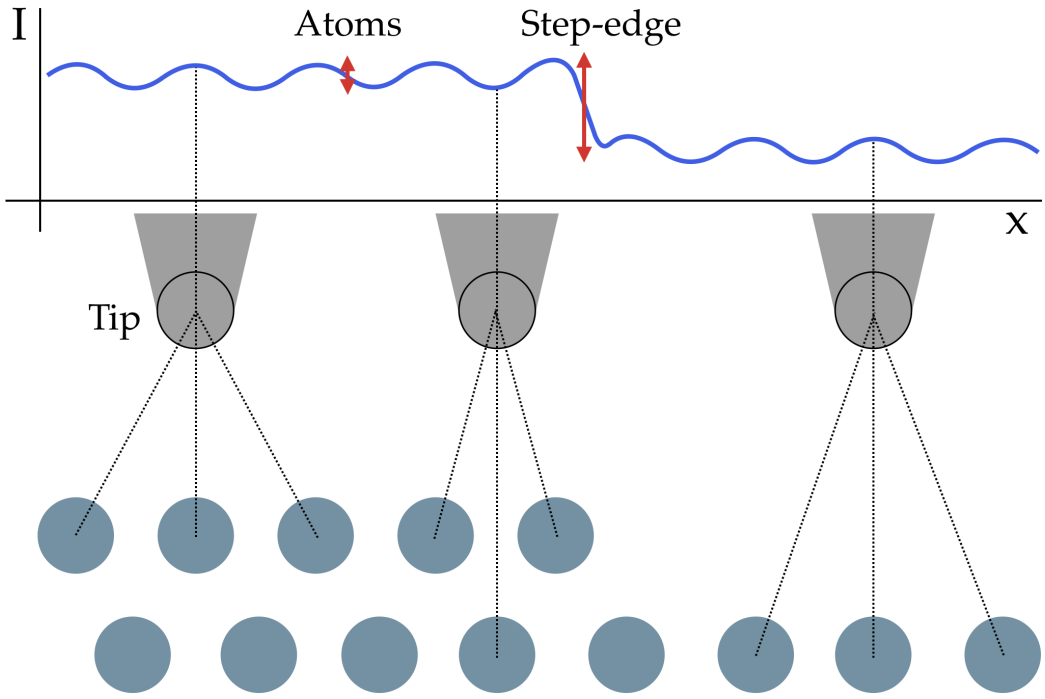

Figure 2.5: *Schematic representation of the measured current when the tip moves past the atoms and the step-edge drawn below. This is a simplified model as we only look in one dimension, moreover, in reality the atoms between layers are not in the same plane. For each tip location the nearest and next-nearest neighbours are indicated. The measured current is a sum of the contributions of all the neighbouring atoms. Since the current decays exponentially with distance, the highest current will be measured when right above an atom (left scenario). Furthermore, the measured current when hovering between atoms of the 1st layer (middle scenario) will be significantly higher, then when those 1st layer atoms do not contribute (right scenario). Therefore, the resolution one needs to distinguish individual atoms (left arrow) is higher than the resolution needed to distinguish two layers (right arrow).*

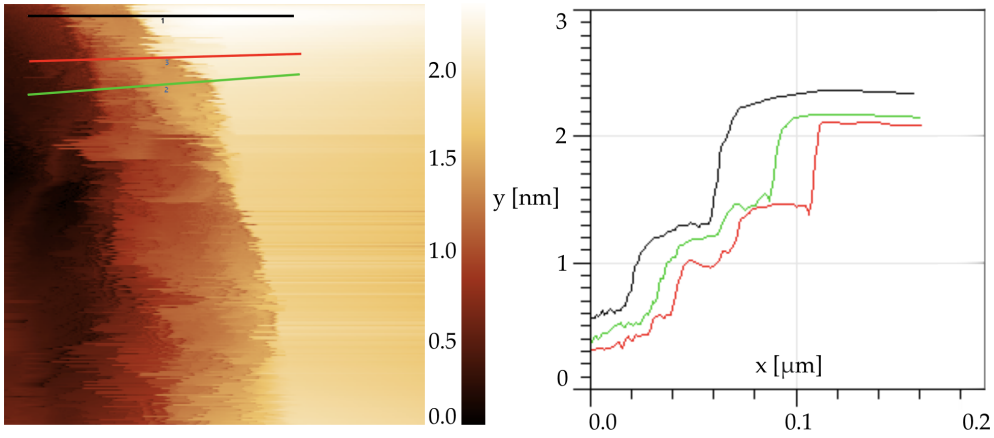

Figure 2.6: *$\sim$ 350 nm $\times$ 350 nm scan by K. van Deelen and M. Stallen with Camera and the Probe-head STM before this research started. This is also the starting point for this research. Notice that height step-edges seem visible, however, visually the resolution does not look good yet. Right: line-plot of the 1D lines on the scan, which seem to consistently show the same step-height, suggesting that these indeed indicate step-edges. Analysed with free and open-source SPM analysis program Gwyddion*

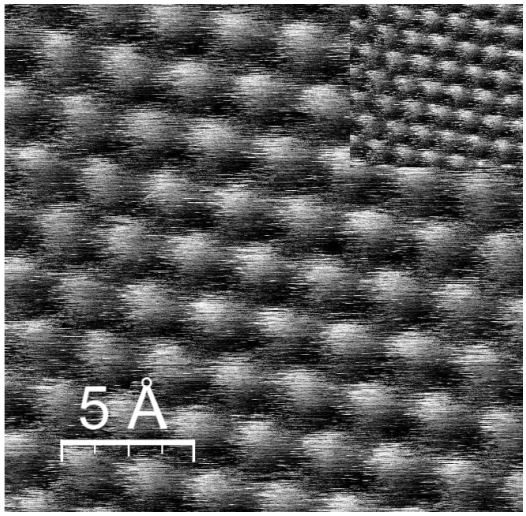

Figure 2.7: *Figure and caption by den Haan et al.in 2014 [12]. "Constant current STM image at 15 mK (2.14 nm x 2.14 nm), showing atomic resolution on HOPG (left to right scan), the right to left scan image is shown in the inset. "*

Spectroscopy

Secondly, we can use STM to do *spectroscopy*. Instead of rastering the tip over the sample, we stay at one specific location, apply a range of different bias voltages V_b on the sample and observe what happens to the tunnel-current I, giving us a I/V-curve. In figure 2.8 we show schematically one of those instances where a certain bias voltage has been applied to the sample, effectively raising the Fermi level of the valence electrons of the sample with respect to that of the tip. The *Fermi level* is the energy level up to which the electrons occupy the available states. States above this level can only be occupied by electrons of higher energy. Since, electrons want to occupy the lowest possible available energy state, the electrons in the sample with higher energy than the Fermi level of the tip will want to tunnel to the tip (fig. 2.8), if allowed. This current is what we call the *tunnel-current*, $I(z)$ in equation 2.1. Now, because the tunnel-current $I(z)$ depends on the amount of electrons within the marked region in figure 2.8, which in turn depends on the LDOS of the sample and tip, measuring this tunnel-current allows us to determine the combined result of the LDOS of the sample and the tip [17]. By choosing a tip that has a constant LDOS at the energy regime where we are measuring, we can assume all the deviations in the I/V-curve are because of changes in the LDOS of the sample. These deviations are more clearly observed in the derivative, i.e. the dI/dV-curve. This way we can use STM to determine the DOS of materials.

We can determine the dI/dV in two different ways. First of all, we can numerically take the derivative of the I/V curve. However, this is prone to noise and error, because we would be numerically taking the derivative of discrete data points. Therefore, the resulting derivative between adjacent points could be very noisy and unrealistically high or low because of noise in the data. To circumvent this there is a second procedure to determining the dI/dV curve, visualised in figure 2.9.

At every bias voltage V_{DC} we slightly oscillate around it at a certain frequency f and amplitude V_{AC}, and measure the tip-current I during the oscillation. Because of the bias voltage oscillating at a frequency f, the tip-current we measure will also oscillate at frequency f. With the lock-in amplifier we can then extract the amplitude of the oscillation of the tip-current I_{AC}. And through relation 2.6 we can determine the dI/dV-curve. Where the approximation of dI/dV becomes better upon choosing a smaller ΔV.

$$dI/dV \approx \Delta I/\Delta V = I_{AC}/V_{AC} \tag{2.6}$$

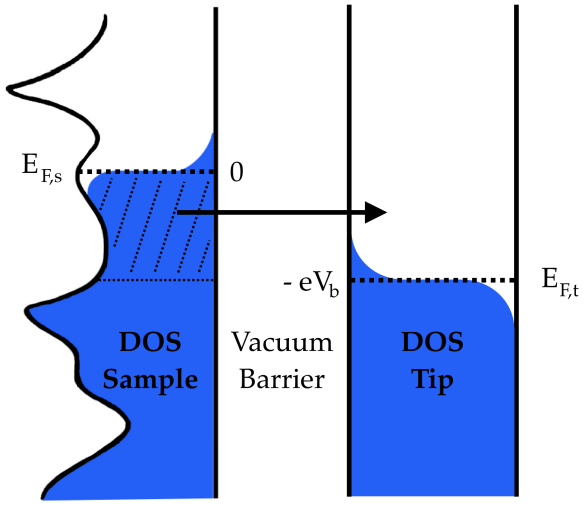

Figure 2.8: *Example of Density of States (DOS) of the tip and sample. On the vertical axis the energy level, on the horizontal axis the amount of different available states for electrons to occupy. With a bias voltage V_b applied on the sample causing the Fermi level of the sample $E_{F,s}$ to shift with respect to the Fermi level of the tip $E_{F,t}$. Blue denotes occupied states. The electrons within the marked area will tunnel from the sample to the tip when the tip-sample-distance reaches tunneling range after approaching.*

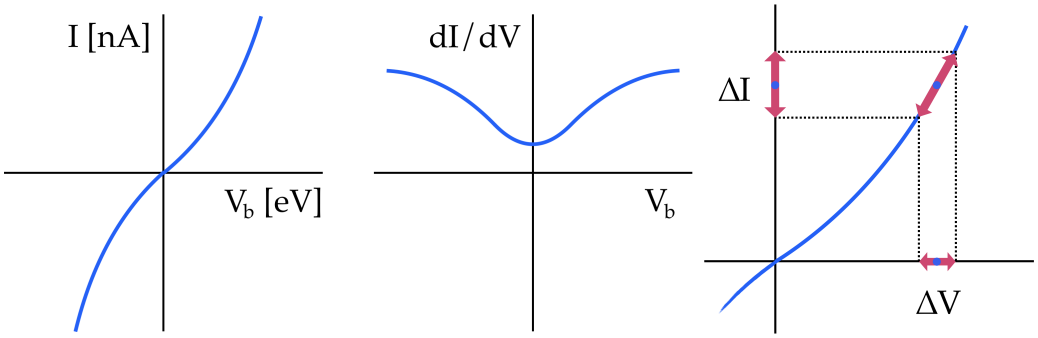

Figure 2.9: *1st & 2nd: Schematic example of I/V-curve and corresponding dI/dV-curve. 3rd: Schematic representation of the second method to determine the dI/dV-curve (sec. 2.2). Oscillate ΔV around a certain bias voltage V_b, and measure the corresponding change in the tip-current ΔI. Then, determine dI/dV following eq. 2.6.*

For spectroscopy the measurement is even more delicate than for scanning. While for scanning we want a certain threshold resolution to observe features qualitatively, for spectroscopy we are more quantitatively interested in the measurement. The stability and precision with which are able to apply the bias V_b and measure the current $I(z)$ is more relevant now. Furthermore, also the temperature of the STM is more important now. The higher the temperature, the less sharp the Fermi work function is, the more the spread we have on features, we call this phenomenon *thermal broadening*. For future research it would be interesting to investigate quantitatively what threshold resolutions we want to aim for, in order to produce high quality spectroscopy. In our group a dI/dV-curve has not yet been produced. This is another goal for the *Oosterkamp Group*. A schematic example of such an I/V-curve and corresponding dI/dV-curve is shown in figure 2.9. Zhang et al. 2016 [33] produced a dI/dV-curve for HOPG, their result is shown figure 2.10.

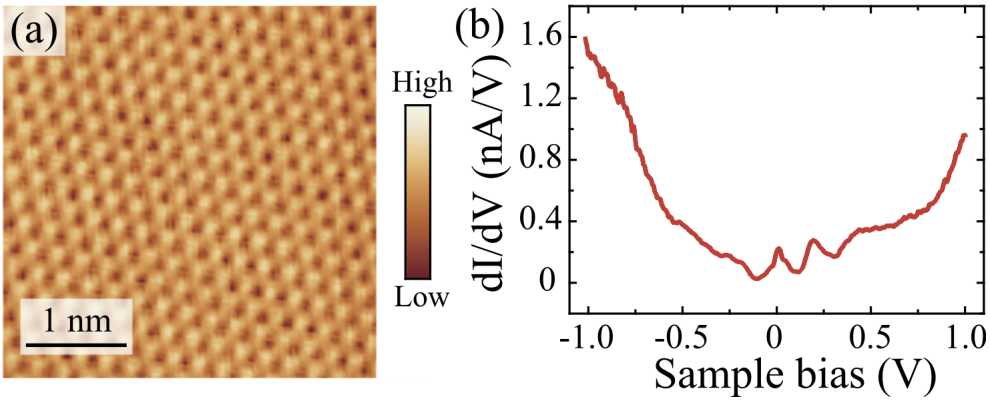

Figure 2.10: *Figures and caption from Zhang et al. 2016 [33]. "Atomically resolved STM image and tunneling spectrum on HOPG surface. (a) Topographic image of HOPG surface with a tungsten tip at 16.8 K. The set point is 0.1 nA / -200 mV. (b) dI/dV spectrum on HOPG with a bias modulation of 14 mV_{rms} at 439.7 Hz. The tunneling gap was set at 0.5 nA -1V before the feedback was turned off.".*

2.3 Cryostat - *Marshmallow*

While the physical principles behind STM are relatively straightforward, the conditions at which we, at the *Oosterkamp Group* are trying to achieve it are challenging. At sub-Kelvin temperatures, while trying to eliminate all forms of noise and vibrations as much as possible. We strive conditions with ultra-cold temperatures, ultra-high vacuum, acoustical-, mechanical- and electrical isolation. For this we make place our STMs into cryostats, which are ^{3}He/^{4}He - dilution refrigerators. A concept that was realized in 1965 in the *Kamerlingh Onnes Laboratorium* at *Leiden University* [8]. After the necessary pre-cooling of the 4K-plate, the further cooling power is caused by the heat of mixing the two Helium isotopes. A schematic representation of the dry dilution system is presented in figure 2.11. On the mixing chamber plate resides the mixing chamber, into which a mixture of ^{3}He and ^{4}He is pumped. Here, a concentrated phase ($\sim$ 100% ^{3}He) lies on top of a diluted phase ($\sim$ 6 %^{3}He). The ^{3}He dilutes as it goes through the phase boundary separating the two phases. This is an endothermic process meaning that it absorbs heat from the mixing chamber. This method allows us to reach milli-Kelvin temperatures on the mixing plate. At the *Oosterkamp Group* we have multiple cryostats. For this research we place our STMs into the *Marshmallow* cryostat, visible in figure 2.11.

Pulse tube vibrations

More specifically, *Marshmallow* is a *dry* dilution refrigerator, meaning that the pre-cooling is done by a pulse tube (PT). Which has the advantage over a *wet* dilution refrigerators in that it reduces the labor intensity of pre-cooling, where helium needs to be refilled regularly [12]. However, the disadvantage of a PT refrigerator is that it pumps at 1.4Hz, causing mechanical and acoustical vibrations. The setup already contains some vibration isolution: all the plates below the Still-plate (1K) are hanging freely in springs. Also, the pumps are attached to a different frame. However, still we expect some of the pulse tube vibrations to enter our system. Therefore, it is necessary to quantify the vibrations caused by the PT, and the resulting effect on our scanning and spectroscopy. To determine the severity of it and what we can do to reduce it. Investigating the noise contribution of the pulse tube is one of the core questions that we will address in this research.

Exchangeable probe

Unique about the *Marshmallow* cryostat, is that there is a cylindrical section cut out through the middle of the plates. This allows for an *exchangeable probe* to be inserted. A component that allows a relatively quick exchange of the experiments and components that are mounted onto to the probe, without having to completely open the entire cryostat and pausing the other experiments. In the absence of a probe and before one can modify an experiment, one has to open *Marshmallow* completely. It has to warm back up, which takes a couple of days to a week. After doing the necessary modifications, the cooling down takes another couple of days to a week. Altogether the cycle can take up to two weeks. This is time-consuming and also hard to manage with the other experiments that might want to continue measuring. This is where the exchangeable probe comes in. The idea is that we can take out the probe, modify the mounted experiments and put the probe back into the cryostat, all while keeping the cryostat under reasonable conditions. The exchangeable probe has been developed by *Leiden Spin Imaging (LSI)* (now part of *Onnes Technologies*) and arrived at the *Oosterkamp Group*, we have tested the exchange mechanism and it functioned as planned. We observed that taking out the probe caused the mixing chamber (MC) plate to increase a couple of Kelvin and we are confident that we can keep the MC plate under 4K. On the other hand, inserting the probe back in caused the MC plate to increase more then 10 Kelvins, depending on how long we kept the probe outside. This could be alleviated somewhat by pre-cooling the prove at the 50K and 4K plates, which are cooled by the pulse tube, which delivers a lot of cooling power. We are working on connecting thermometers inside the probe to monitor the pre-cooling process. We have not yet used the probe for the exchange of experiments.

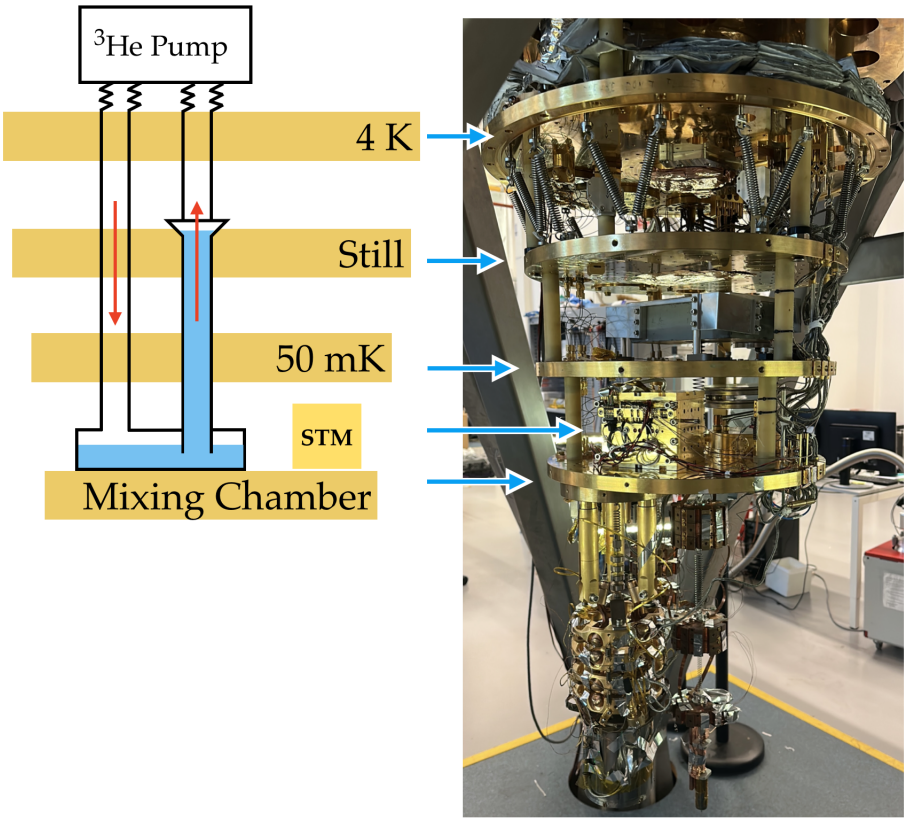

Figure 2.11: *Left: schematic representation of the lowest four plates and the dry dilution system. Right: 'Marshmallow' the dry dilution refrigerator when opened, i.e. the radiation shields and vacuum chambers are not attached.*

Chapter 3

Methods and Implementation

This chapter covers the methods and specifics of our set-up in order to strive for quality measurements. We start by describing how we prepared our tips and samples. Followed by an explanation about how we approached our tip to the sample without crashing the tip. Finally, we map out the different noise and interference sources and explain what measurements we can do in order to analyse the contribution of the pulse tube.

The *Oosterkamp Group* develops two STMs, which are named *Basic-STM* and the *Probe head (PH) STM*. Both STMs have different advantages and disadvantages over each other. The PH-STM is much smaller and would fit into the exchangeable probe, that can be inserted into or removed from the cryostat, which makes it more flexible to use and adjust without disrupting the other experiments in the cryostat. On the other hand, the Basic-STM makes use of the new *'Linear Cryo-Walker'* motors from *Onnes Technologies* which have advantages over the *stick-slip-motors* that will be discussed in section 3.2. The other parts of the setup, like the tip, sample and electronics are essentially the same. By developing two STMs, that slightly differ from each other, the *Oosterkamp Group* has two chances to make it work. In this thesis we focus on the implementation and results of the Basic-STM.

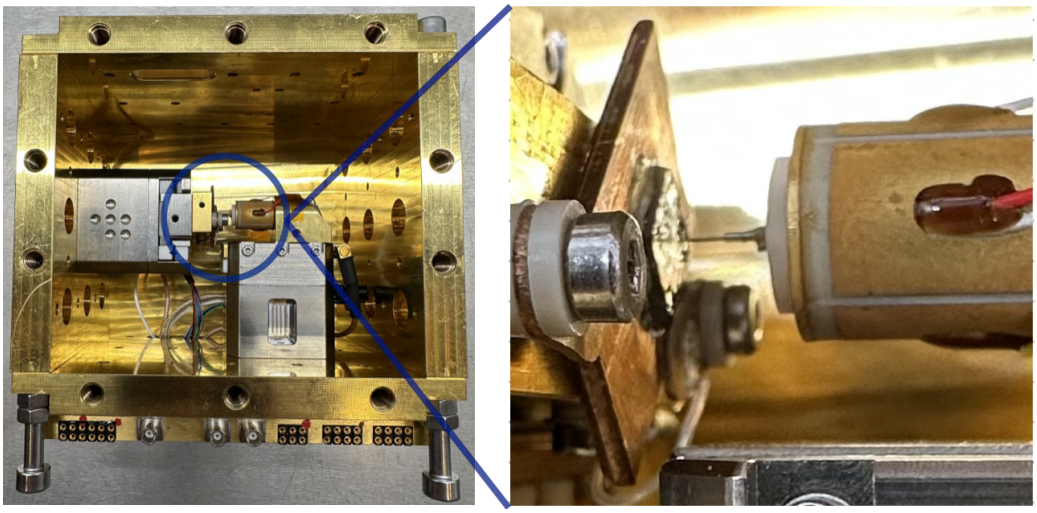

Figure 3.1: *The Basic STM setup is mounted onto gold-plated copper that serves as electrical shielding against the other experiments in the Marshmallow cryostat. Schematics of the Basic STM are shown in fig. 3.3.*

3.1 Tip and sample implementation

We start by explaining how we make our tips and how to treat a tip in-situ. Furthermore, we discuss a possibly new method to etch significantly sharper tips. Lastly, we explain how we prepared our samples.

Tip preparation

As explained in section 2.1, to achieve atomic resolution, it is required that we have a tip that is as sharp as possible. Preferably one atom thick, although this is incredibly hard to achieve [5]. For this research we chose to make Tungsten (W) tips. This, because we know that it has a relatively flat density of states, which is desired because then we can use it to determine the density of states of our sample as explained in section 2.2. Also, Tungsten is relatively rigid which makes it less sensitive to vibrations and easy to etch.

We made tips with 0.5mm⌀ and 0.25mm⌀ Tungsten wire. We started with preparing the wire by sanding it with Scotch-Brite to sand off the oxidation, cleaning it in a 50/50 mixture of isopronanol and acetone, followed by putting it in the sonicator for roughly 3 minutes. Then, we produced

our tips according to the *lamellae drop-off method*, where we electrochemically etch the Tungsten wire. A schematic representation of our setup is shown in figure 3.2. We clamp the Tungsten wire and run it through a wire guide that prevents the wire from sticking out in random directions. By dropping a little amount of the basic solution on a small loop, which the Tungsten wire penetrates, a small meniscus is formed inside the loop that encloses the Tungsten wire. For this research we used a basic solution of NaOH in water. We produced this solution by dropping 80 NaOH pellets (0.1 g/pellet) inside 40 mL of demineralized (demi) water, gradually adding the pellets to prevent overheating. After about 20 minutes the pellets were completely dissolved into the water. The molar masses of H_2O and NaOH are about 18 and 40 g/mol and 40 mL of H_2O weighs 40 g. Thus, we have 2.22 mols of water molecules and about 0.2 mols of NaOH molecules. This means our basic solution contained about 9% of NaOH. The length of the tip is determined by the amount it sticks out under the meniscus. For this research we made tips of approximately 5-10 mm. Then, by applying a $\sim$3.3V between the loop (cathode) and the Tungsten wire (anode), the Tungsten wire will start to *etch* away at the place where the meniscus meets the Tungsten wire. According to the chemical reaction as described in Ibe et al. (1990) [13]. This happens slowly and takes about 10-15 minutes, depending on the initial thickness/diameter of the wire, until the part inside the meniscus is etched away and the connection breaks. This fallen wire, now with an extremely thin apex, is our tip. We chose this orientation because we think this way we also have the benefits of gravity pulling the apex even thinner in the last seconds before the connection breaks. However, we are not certain about this, as we are not able to optically validate this assumption. When it falls we need to catch it softly without touching the apex in order not to ruin it. For this, we place a glass cup filled with shaving foam under the location where the tip will fall, because shaving foam is very light and easily compressible. This way the tip falls into the shaving foam with the apex sticking out, and not touching anything.

$$\begin{aligned} \textit{Cathode} \quad & 6\,H_2O + 6\,e^- \longrightarrow 3\,H_2(g) + 6\,OH^- \\ \textit{Anode} \quad & W(s) + 8\,OH^- \longrightarrow {WO_4}^2 + 4\,H_2O + 6\,e^- \end{aligned}$$

$$W(s) + 2\,OH^- + 2\,H_2O \longrightarrow {WO_4}^2 + 3\,H_2(g)$$

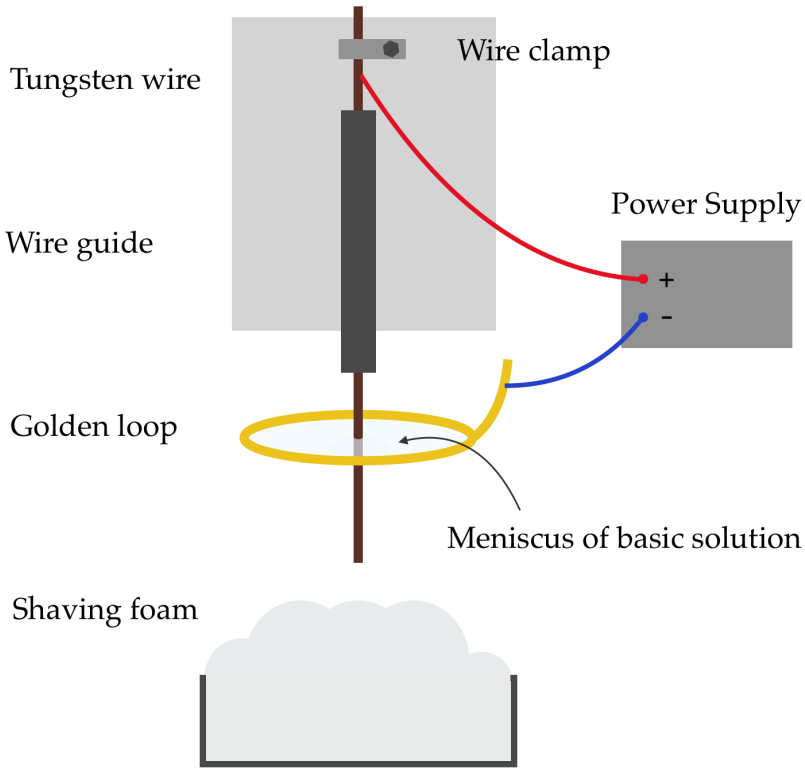

Figure 3.2: *Schematic representation of our tip-etch setup.*

After we produced a tip, we picked it up with inverted tweezers and cleaned it by dipping it into a 50/50 mixture of isopropanol and acetone, dipping it into water and blowing the excess of with the compressed Nitrogen gun. When we dipped our tip into any of the liquids we made sure to dip the tail of the tip first such don't break the surface tension of the liquid with the tip apex, which risks blunting the tip. When a tip was properly cleaned, we stored it in desiccator that is filled with Nitrogen. This helps prevent oxidation and with that extends the life-time of our tips.

Tip treatment in-situ

Even if we set-up a 'perfectly' sharp and clean tip onto the STM and into the cryostat, this does not ensure a good tip throughout the operation. Many things can cause the tip to blunt or contaminate and deteriorate. If necessary, there is a local smoothening method at our disposal, developed by Feenstra et al. (1987) [11]. We apply a large enough bias voltage V_b to the sample, generating a field-emission current at the tip, that will cause the apex to melt [7] and a new apex is formed, hopefully yielding better results. One can do this until a stable I/V-curve is observed. The melting will cause local damage to the sample, which is why it is advised to move the tip to an unused area of the sample before starting this procedure.

Tip method discussion

According to Bowen Li et al. (2019) [5], through the conventional DC electrochemical etching method it is difficult to produce tips with radius smaller than 100 nm. Furthermore, they propose that the *double-electrolyte etching method* is an efficient method to produce smaller tips. More than half of the produced tips were smaller than 50 nm. They even produced tips with 8mm radius. This is further supported by Yingzi et al. (2018) [19], who also implemented this method, and obtained 40% of the fabricated tips to have 20-40 nm diameter and 30 % below 20 nm diameter. We expect that having smaller tips increases the odds of having an atomically sharp tip. Additionally, the capacitance between the tip and the sample C_2 in figure 3.5 will become greater and a greater capacitance could contribute to reduction of the voltage-noise across the junction, and with that the effective temperature of the STM. This method might be interesting for the *Oosterkamp Group* as well to implement. However, at this stage of our STM development, the tips have to be *good enough* to distinguish the features, which they are. Improving the tips is therefore something further on the agenda. Therefore, we have not implemented this method for this research.

Sample preparation

The process for preparing our sample is less rigorous then preparing the tips. And that is also because we use a relatively easy and forgiving material, namely, Highly Oriented Pyrolytic Graphite (HOPG). As explained in Patil et al. (2017), HOPG consists of layers of carbon atoms that are weakly bonded together by the van der Waals force. A single 2D layer of carbon

atoms is called graphene and can be considered as one atomic layer of graphite [23]. Graphene has a hexagonal structure of carbon atoms with two lattice constants of $|a_1| = |a_2| = 2.46$Å [16], that represent the distance between nearest neighbours in the lattice. The distance between two layers is about 3.35 Å [24]. The weak van der Waals bonding between the layers allows us to easily produce a clean and atomically smooth surface by cleaving HOPG, making HOPG a commonly used sample for STM measurements [6]. Also, HOPG is relatively inert, does not react with Oxygen and materials do not stick to it, keeping the HOPG clean. Furthermore, the properties of HOPG are well known, therefore we can use it to benchmark and calibrate our set-up, before trying other materials. To cleave HOPG, we stick Scotch Tape onto a piece of HOPG and peel it off. Because of the weak van der Waals bonding between the layers, we peel of a couple of layers of HOPG, leaving us with a clean layer of HOPG. We did this a couple of times until the surface looked clean. Which we assumed to be the case if we observe a single reflective layer without interuptions. Then, we looked at it under a microscope to see if we indeed have a clean surface. Whenever something happens that damages our surface, we can peel of a couple of layers and obtain a clean surface again.

3.2 Approaching

Before being able to do *scanning* or *spectroscopy* with our STMs, the tip has to be within tunneling range of the sample. The process of bringing the tip carefully close to the sample is what we call *approaching*. Approaching is a delicate process because we need to move the tip incredibly close to the sample, in the order of Ångströms (0.1 nm), while the tip could start at a distance of 1mm, without crashing it. Crashing could blunt the tip and requires the production of a new one. Approaching consists of two phases: the *coarse-approach* and the *fine-approach*. During the coarse-approach we brutally take steps, without sensing if we are near the sample. During the fine-approach, before we take a step, we extend the scan tube to sense if the sample is near. And only if it is not, we take a step.

For the *Basic-STM* we are able to move the tip by attaching the scan tube to *cryo-walkers* produced by *Onnes Technology*, as shown in figure 3.3. The walker can take steps at ultra-low temperatures that are smaller than a micrometer. The walking mechanism is visualised in fig. 3.4. The walker consists of 2 'legs', each have a pairs of lift piezos with a shear piezo in between. 1 step is taken by first extending 1 of the lift piezos and extending the other (lifting 1 foot), and then deform the shear piezo (depending on the walk direction), and lastly extend/contract the lift piezos back (putting the foot back on the ground). This is repeated for the other 'leg', such that 2 steps completes a walk cycle.

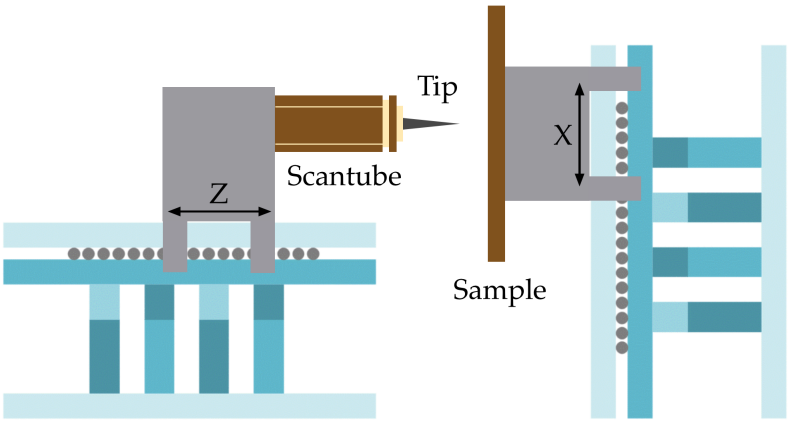

Figure 3.3: *Schematic representation of how the tip and sample are connected to the Onnes-cryo-walkers. Notice that the scan tube and sample holders are attached to the darkblue slider and not to the lightblue part which is there to apply a counter pressure. Schematics of the cryo-walkers are from Onnes Technologies [26].*

Getting the cryo-walkers to walk properly is challenging because a sweet spot has to be found within a large parameter space. The motor contains 9 tuneable parameters, 4 'Amp' parameters, 4 'Off' parameters and 1 'Shear' parameter, that determine the voltage put on each of the piezos in the *cryo-walkers* from fig. 3.4. Furthermore, the parameters differ for different types of movement. Approaching and retracting differ, the Z-motor and X-motor also differ from each other and a change in temperature also changes the parameters. For these reasons, we suggest tuning and checking the parameters every time before one aims to walk with the motors. We did this by choosing the maximum allowed voltage for each parameter, and then decreasing the parameters individually as much as possible until performance start to drop drastically. However, some values only work in combinations. This requires a lot of trial and error. Currently, in cold conditions we are able to approach and retract the Z and X motor with parameters below. These values where found together with David Coffey, the application scientist of *Onnes Technologies*. 80V on the lifts was enough to move at room temperature, but we saw no movement when cooling down. It turned out that it was critical to also retract (negative offset) the other lift piezos when taking a step. This gave just enough space for the walker to take steps.

$$\begin{aligned} Amp &: AA, AB, BA, BB = 80, 80, 100, 100 \\ Off &: AA, AB, BA, BB = 70, 70, -80, -80 \\ Shear &: 320 \end{aligned}$$

The new cryo-walking technology is an improvement to the older *stick-slip* mechanism, that is present in the probe head (PH) STM. One of the benefits can be seen in figure 3.4, the *legs* can actively make and break mechanical connections with slider, while the slip-stick mechanism relies on friction [26]. This friction turns into heat and too much heat is undesired in our aim for ultra-low-temperature conditions. 1 minute of full speed movement caused heating from 100 mK to 2 K, which is highly undesirable when working in a shared fridge, possible ruining the experiments of our colleagues. Another benefit is the capacitance-based position sensor of the walker which we can use to determine if the slider is moving.

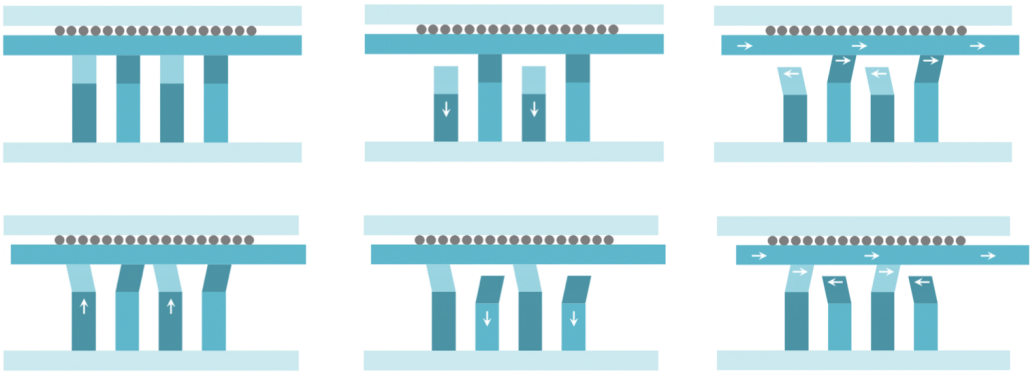

Figure 3.4: *Figures from Onnes Technologies [26]. The cryo-walking mechanism in the Onnes-motors. The walker contains 'lift-piezos' that extend and contract in the lateral direction, indicated by the vertical arrows. And 'shear-piezos' that deform in the horizontal direction, indicated by the horizontal arrows. The time-line is from left to right and then from top to bottom. First: legs 1 and 3 shrink and legs 2 and 4 shear. Then, legs 1 and 3 extend back. Next, legs 2 and 4 shrink and legs 1 and 3 shear. Then, legs 2 and 4 extend back. The process repeats. The lift piezos are attatched to the motor casing (light blue), which stays still at all times. The slider can move along ball bearings with respect to the motor casing, and is pressed tightly between the piezo legs and the casing by a spring. By attaching the scan tube or sample to a slider as shown in figure 3.3, we can move it precisely.*

As mentioned, approaching consists of two phases: the coarse-approach and the *fine-approach*. During both phases we only take steps with the walker to which the tip is attached, i.e. the left walker in figure 3.3. The coarse-approach is characterized by manually taking steps that bring the tip closer to the sample without actively checking if they will crash before taking a step. One only does this in regions for which the sample is not near. To evaluate how close the tip is to the sample we follow the procedure developed by de Voogd et al. [31], who suggested that the absolute tip-sample capacitance shows generic behaviour as a function of the distance, independent of the tip. Namely, we can view the absolute tip-sample capacitance as the contribution of two different capacitors connected in parallel, the capacitance between the tip-holder and the sample C_1 and the capacitance between the tip and the sample C_2, as can be seen in figure 3.5. Now, because a capacitance depends on the distance d between the two plates as well as the area A of each plate, through: $C = \epsilon A/d$, with ϵ the permittivity of the vacuum between the plates. The contribution to the total capacitance of C_2 will only become relevant when the tip approaches near tunneling range. Whereas up to that point C_1 was dom-

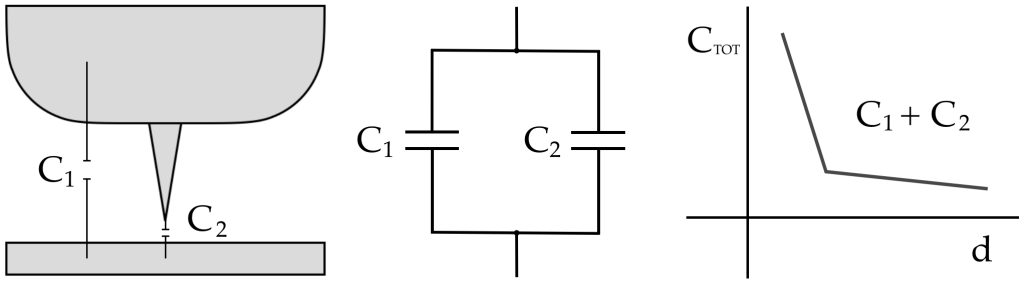

Figure 3.5: *We may view the total absolute tip-sample capacitance C_{TOT} as the combination of the capacitance between the tip-holder and the sample C_1 and the capacitance between the tip and the sample C_2 connected in parallel. Because of the different geometries and materials of the components C_1 and C_2, the relative contribution to C_{TOT} will depend on the distance d between the tip and the sample. While C_1 will dominate for the most part, at some point the contribution of the tip C_2 will start to dominate. This is the indication to start the fine-approach.*

inating. And because the dimensions of the tip and the holder, and thus the dependence of A on d are so different, the slopes of the capacitance vs. distance will differ. During the coarse-approach we monitor this total tip-sample capacitance using the *lock-in amplifier* we mentioned in sec. 2.1. By applying an AC bias to the sample at a specific frequency, and measuring the transmitted signal at the tip, we can deduce the capacitance. A sudden increase of the slope indicates that we are near the tunneling range and that it is time to start the fine-approach. A schematic example of the change of slopes that we would expect is shown in figure 3.5. However, in practice we approached our tip manually, by eye, close to the sample and then started the fine-approach immediately, which takes significantly longer. Because we have not yet investigated what capacitance indicates the change of slopes, or set-up a system to clearly indicate the change of slopes.

While the coarse-approach is done manually, the fine-approach is completely automated and run digitally by an *Scanning Probe Microscopy (SPM)* controller. In our case we started with the completely analog controller called *Camera*, but we were happy to temporarily use *Nanonis*, which is digital and more user friendly (built in scopes, full parameter control, such as scan tube Z-voltage). The program controls when to *sense* and when to take a step. Before it takes a step it senses whether the tip is in tunneling region. Sensing is done by slowly ramping up the voltage on the Z-piezo of the scan tube. This will cause the tip to gradually extend. During the sense it keeps track of the tip-current. If at some point it measures a tip-

current above a certain threshold (in our case around 100 pA - 1nA), the scan tube immediately retracts the tip and the SPM controller announces that the tip has 'approached'. It will not take a step anymore, because this would result in a crash of the tip. If during the sense it does not measure a tip-current it will proceed by taking a step forward after which a new sense will start. This procedure repeats until the tip is approached. The advantage of the fine-approach is that the tip should never crash into the sample, if a coarse-step is smaller than the range of a sense. We made sure that a coarse step never exceeds half the sense range. The disadvantage is that it takes much longer since it has to sense before every step. In this research the full sense - extending and returning to initial position - was set to take about 0.5-2 second. But, one can change the duration of a sense to any value, as long as it is not too fast. After the tip has successfully approached the sample can be scanned, or spectroscopy can be performed, with the SPM controller. In building, testing and calibrating the STM we were glad to be able to borrow an SPM controller called *Nanonis*, as it is more user friendly and shows all signals such as the current, the out-put of the lock-in amplifier, etc. live through time and is therefore easier to learn from. However, our group does not yet own a *Nanonis* setup yet. We could only borrow it and this was not always possible.

3.3 Noise, interference and how to analyse the pulse tube contribution

In this section we want to map out the different sources that we are dealing with. Furthermore, we will explain how we are going to analyse the contribution of the pulse tube and why we are interested in investigating the pulse tube in the first place.

If the previous steps are completed successfully, i.e. we are measuring a tunnel-current with a clean tip and sample, without having crashed the tip, we are ready to do measurements. At this point, the resolution of our setup depends upon three factors. First of all, how precise we are able to apply our bias voltage V_b, where the DC-component is generated by the SPM-controller and the AC component is generated by the lock-in amplifier. Secondly, how precise we are able to measure our tip-current $I(z)$ using the DAQ. And lastly, how much noise there is in the system. As will become clear, currently the noise and interference sources are the limiting factors. To this end we want to map out the different noise and interference sources to investigate the severity and determine what we can do to improve it.

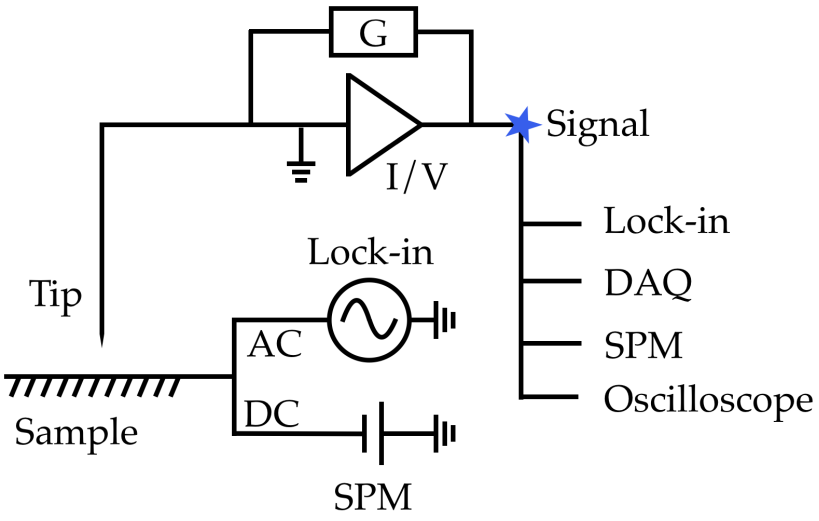

Figure 3.6: *Simplified schematics of the electrical circuit of the STM. Excluded is for instance the scan tube.*

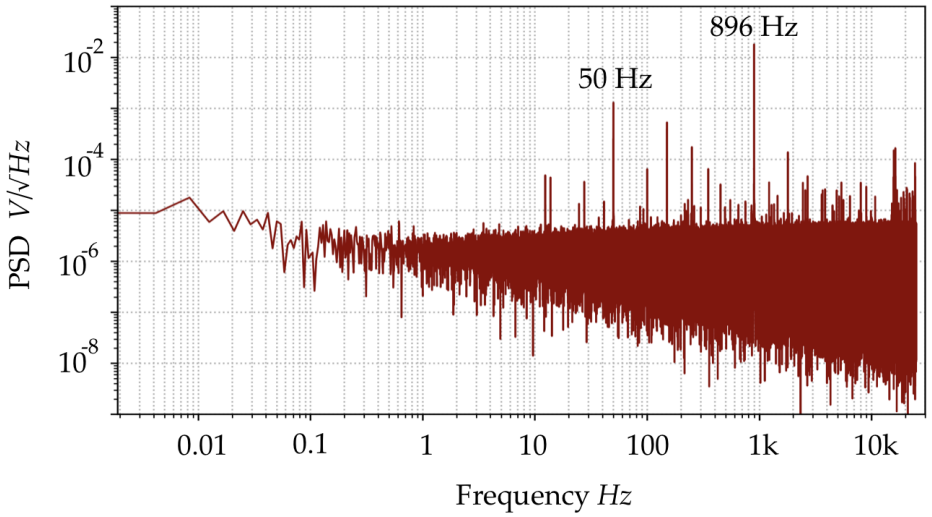

Figure 3.7: *Fourier transform of the bias voltage V_b, with AC component at frequency $f = 896Hz$ with amplitude 1 mV and DC component of 1 V. Notice that the noise floor lies around $10^{-7}V/\sqrt{Hz}$, significantly lower than our signal when doing measurements, fully connected and in tunneling range (fig. 4.1). Therefore, at this point, we do not worry about the noise contribution from generating a bias.*

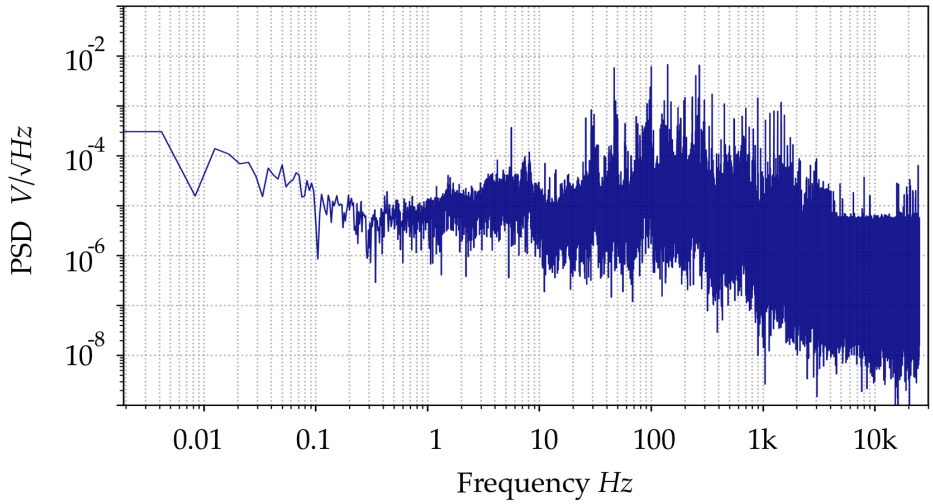

Figure 3.8: *Fourier transform of the tip-current at room temperature, out of tunneling range, with pulse tube off. The noise floor lies around $10^{-6} - 10^{-7}V/\sqrt{Hz}$. However, a significant amount of 50 Hz enters our system, a noise source that we would like to reduce.*

Noise and interfering sources

The noise on the tip-current has a couple of contributions that are well known. First of all, the *Femto DLCPA-200* I/V-converter contributes a noise floor of:

$$\begin{aligned} S_{FEMTO} &= 4.3 fA/\sqrt{\text{Hz}} \ \ [9] \ \ (\text{up to 1 kHz}) \\ &= 4.3 \mu V/\sqrt{\text{Hz}} \end{aligned}$$

Where in the last line we applied the $\times 10^9$ gain. Generally, we always measure voltages, meaning that whenever we are talking about a current noise, we have measured a voltage and applied the gain to convert it to a current. Looking at the current noise caused by the I/V-converter we now know that whenever we analyse a tip-current in the Fourier domain (section 4), the noise floor should be at least, at 10^{-6} line. This serves as a sanity check as well. Additionally, we have a contribution due to the discrete nature of electrical charge, called *shot noise* [15]. For a tunnel current at 1 nA this is given by:

$$\begin{aligned} S_{I_{shot}} &= 2eI_0 \\ &= 2 \cdot 1.6 \cdot 10^{-19} \cdot 10^{-9} \ \text{A}^2/\text{Hz} \\ &= 3.2 \cdot 10^{-28} \ \text{A}^2/\text{Hz} \\ &\rightarrow 1.8 \cdot 10^{-14} \ \text{A}/\sqrt{\text{Hz}} \\ &= 18 \ \text{fA}/\sqrt{\text{Hz}} \\ &= 18 \ \mu\text{V}/\sqrt{\text{Hz}} \end{aligned}$$

Where, $e = 1.6 \cdot 10^{-19}$C is the elementary charge, $I_0 = 10^{-9}$A is the tip-current which for our STMs is of the order of a nanoampere (nA). Notice that the shot noise is higher than the noise floor of the I/V-converter. This is a positive thing, because this means that we are in principle able to measure the shot noise, which is also one of the goals at the *Oosterkamp Group*.

Next, we have the thermal noise (or Johnson noise) naturally caused by the resistance of an electrical component. It is constant for every frequency, also called white noise, up to a certain cutoff frequency f_c [32]. The individual components and resistances will contribute to this, but we have not investigated exactly which components this includes. But, as we will show: a rough estimate suggests that this source of noise will not be the first of our concerns. Looking at eq. 3.1, we observe that the total

noise is linearly proportional to the temperature, as well as the resistance. Since the resistance of electrical components drops with decreasing temperature, we assume that the contribution to the noise of the components at room temperature will be leading over that of the ultra-cold components. Thus, we think it is acceptable to only look at the room temperature contributions for now.

$$\begin{aligned} S_{V_{R@T_{room}}} &= 4k_B TR \\ &= 4 \cdot 1.38 \cdot 10^{-23} \cdot 293 \cdot 3 \text{ V}^2/\text{Hz} \\ &= 4.85 \cdot 10^{-20} \text{ V}^2/\text{Hz} \\ &\rightarrow 2.2 \cdot 10^{-4} \ \mu\text{V}/\sqrt{\text{Hz}} \end{aligned} \tag{3.1}$$

Where, $k_B = 1.38 \cdot 10^{-23} J \cdot K^{-1}$ is the Boltzmann constant, $T = 293K$ is room-temperature and $R = 3\Omega$ is the resistance of 10 meters of BNC cable (save overestimation). And we measured 1 meter of BNC to have a resistance of $\sim 0.3\Omega$. Notice that this contribution is four orders of magnitude smaller than the contributions of the I/V-converter and the shot-noise. The total resistance of the components should be 4 orders of magnitude higher, i.e. 10.000 Ω instead of the currently approximated 1Ω, to start being relevant. Hence, for now this noise source is not our first concern.

Of the noise sources above, we know roughly the height of the noise floor and there is no way around it. But, we also have sources with a lesser known noise floor. For instance, the components of the STM have a certain temperature and therefore radiate. Which with a temperature of 10 mK would correspond to about 1 GHz of radiation through $k_b T = hf$. Where, $h = 2.63 \cdot 10^{-34} J \cdot s$ is the Planck constant. However, it should be noted that the heat dissipation at these temperatures is not as straightforward. Next to that, we have thermal noise due to the *effective electron temperature*. Even though our tip and sample can reach sub-Kelvin temperatures, the electrons that tunnel through the tip-sample junction started their journey from outside the cryostat, at room temperature. Meaning that they will not have necessarily reached the sub-Kelvin temperatures of the tip and sample, causing thermal noise. There is a whole branch of research dedicated to quantifying this effect and determining how to minimize the consequences of it. In this research we do not delve into this matter. Another important property of the system that in future research we would like to quantify is the piezo creep of the piezo electric components in our setup, such as the scan tube or the linear cryo-walkers that we use for coarse movement of the sample and tip.

Furthermore, we have *interfering sources* to which we dedicate great effort in order to decrease the contributions. These interfering sources include *mechanical*, *radiation* and *acoustical* interference. The pulse tube is one of the sources that contributes mechanical and acoustical interference.

Pulse tube contribution analysis method

We expect that the pulse tube vibrations are one of the prominent noise sources as during operation at milli-Kelvin temperatures the pulse tube is pumping Helium back and forth at $\sim$1.4 Hz, causing vibrations. Therefore, it is valuable to quantify the contribution and determine the severity. The pulse tube pumps at 1.4Hz and is physically connected to the cryostat. This will cause mechanical and acoustical vibrations, of which we think former is dominating. The cryostat has vibration isolation, but is it effective enough at reducing the 1.4Hz vibrations caused by the pulse tube? Because if not, the STM might need its own mass-spring system to reduce the vibrations caused by the Pulse tube even more. We want to find out the magnitude of the oscillations, as well as the location where the vibrations enter the system.

We expect that the pulse tube vibrations enter the tip-current circuit at the tip-sample, because the tip and sample will vibrate relative to each other, and at the input of the the I/V-converter through microphonics: vibrations inside a coax cable results in a changing self capacitance which results in an oscillating current. This current will also be amplified and present in our signal. Then, through the feedback-loop the oscillations will always effect the tip-current, and with that the position of the tip. This will cause oscillations at 1.4Hz and its multiples, with a certain amplitude, which eventually cause an uncertainty in our measurements and reduces our resolution. We are interested in this amplitude because we can compare it to the resolution we want to achieve (section 2.2) to see whether it is negligible or not. In order to investigate this, we make little changes to the setup and observe what effect it has on the spectrum of the tip-current. We measured the tip-current in the various cases listed below:

- Different bias voltages V_b while keeping the set-point constant
- With or without feedback at a certain set-point
- In or out tunneling-range

Then, by analyzing the data in the Fourier domain allows us to draw conclusions. In the next section we will investigate the contributions and

features at 1.4Hz and the multiples of 1.4, both qualitatively and quantitatively, and compare the different measurements. For the quantitative analysis we compute the *Power Spectral Density* which shows the power distribution at each frequency [4]. The area under a curve then gives the power contribution of a certain frequency component, such as the contributions of the Pulse tube at 1.4Hz and its multiples. Furthermore, we will explain how we can relate the power in the vibrations to the physical amplitude of the tip-sample distance and the corresponding impact on the resolution. Finally, we want to put this into perspective by comparing it to the desired resolution, the values we find in literature and the value we would expect if we model the STM as a mass-spring system.

Mass-spring model of pulse tube vibrations

As we discussed in the previous section, we expect the vibrations of the pulse tube to enter through microphonics or the changing tip-sample distance. We can already quantify the expected vibrations caused by the changing tip-sample distance. And use this value later to compare it with what we measure. We relate the Z-motion of the plate that the STM is mounted on to the motion of the tip, by modeling the STM tip as an effective mass m_{tip} that is connected to the body of the STM with an effective spring constant κ_{STM}. The STM has an internal resonance frequency of:

$$\omega_{STM} = 2\pi f_{res} = \sqrt{\frac{\kappa_{STM}}{m_{tip}}} \tag{3.2}$$

that is typically 1 kHz for a stiff STM and can be as high as 10 kHz for a very stiff STM, according to *Prof. dr. ir. Tjerk Oosterkamp*. Then, when the plate onto which the STM is mounted accelerates upward because of the vibrating pulse tube at 1.4 Hz, there must be force on the effective mass that we call:

$$\begin{aligned} F_{tip} &= m_{tip} \cdot a_{tip} \\ &= m_{tip} \cdot \omega^2 A_{plate} \end{aligned} \tag{3.3}$$

Where, A_{plate} is the amplitude of the up-down motion of the Mixing Chamber (MC) plate onto which the STM is mounted. Which according to *Prof. dr. ir. Tjerk Oosterkamp* is around 1-10 μm at 1.4 Hz. Now, by modeling the the STM tip as an effective mass connected to the body of the STM, this force must come from the stiffness of the STM. So, we have:

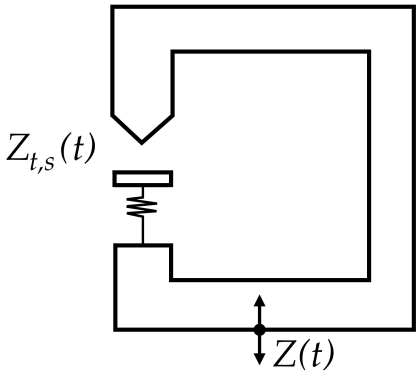

Figure 3.9: *Schematics of modeling the STM as an effective mass that is connected to the body of the STM with an effective spring constant.*

$$\begin{aligned} F_{tip} &= \kappa_{STM} \cdot x_{tip-sample} \\ &= m_{tip}\omega_{STM}^2 \cdot x_{tip-sample} \end{aligned} \tag{3.4}$$

Where substituted eq. 3.2. Now, by equating eqs. 3.3 and 3.4 and simplifying the terms we arrive at:

$$x_{tip-sample} = A_{plate} \cdot \frac{\omega^2}{\omega_{STM}^2} \tag{3.5}$$

We can fill in eq. 3.5 using the boundary values for A_{plate} and ω_{STM} to obtain a worst case and best case scenario. In the worst case, we have a not so stiff STM with $\omega_{STM} = 1kHz$ and an amplitude of the up-down motion that is $A_{plate=10\mu m}$. This results in the tip-sample distance to be $x_{tip-sample} = 0.2$Å. In the best case we have a very stiff STM with $\omega_{STM} = 10kHz$ and an amplitude of the up-down motion that is $A_{plate=1\mu m}$. This results in the tip-sample distance to be $x_{tip-sample} = 0.0002$Å. Therefore, we suggest that:

The pulse tube is expected to cause the tip-sample distance
to vibrate between $0.0002 - 0.2$Å

Chapter 4

Measurements, Results and Discussions

This chapter presents and discusses the results of various measurements conducted with the *Basic-STM* at room temperature and at ultra-low temperatures. At ultra-low temperatures the STM will experience vibrations due to the pulse tube pumping of He4 back and forth, which is necessary to achieve sub-kelvin temperatures. We expect this to be the main cause of mechanical vibrations at low frequencies, and that it could stop us from achieving atomic resolution. We present analysis of tip-current spectra, centered around investigating the contribution of the pulse tube, while varying the bias voltage, with or without feedback and in or out tunneling regime. The motivation for varying these variables is explained in sec. 3.3. Finally, we present our scanning results.

4.1 Ultra cold spectra analysis Varying biases (in tunneling)

We are interested to know what the effect of the pulse tube (PT) is. Is it present in the spectrum? And where does it enter the circuit? How is it effected upon changing the setup such as changing the tip-sample distance? And what power does the PT contribute to the total noise? To this end, we measured the tunnel-current with different bias voltages V_b, while keeping the set-point constant at 100 pA. A constant set-point means that increasing the bias effectively means decreasing the tip-sample distance. All these measurements were done in tunneling regime. For each V_b we measured in feedback and with the feedback frozen. By freezing the feedback we

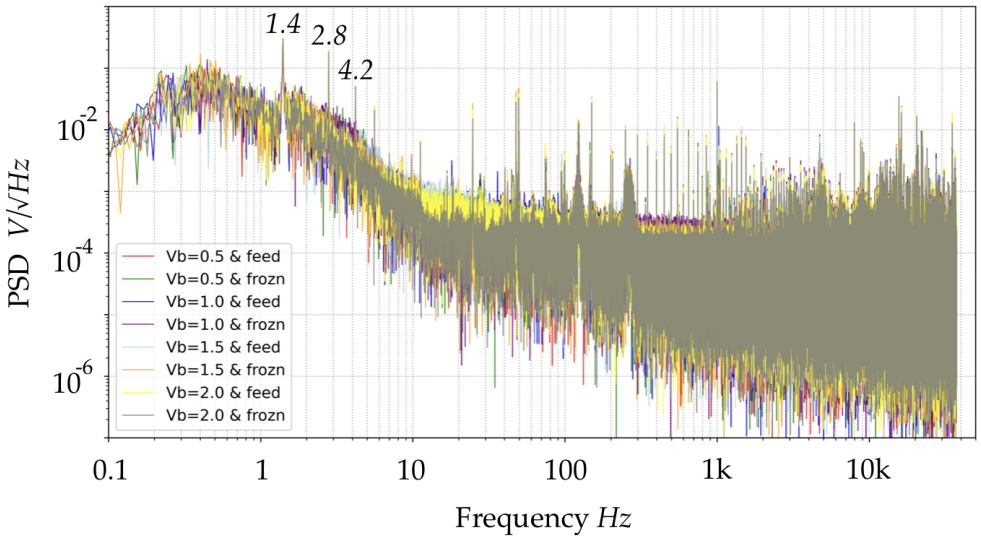

Figure 4.1: *Fourier spectra of the tip-current for different bias voltages V_b and with feedback on/off. The multiples of the pulse tube are clearly visible. All measurements were done in tunneling regime. 50 Hz peaks are also visible.*

are able to observe the raw contribution of the pulse tube. And with feedback on, we the peaks of the pulse tube to be reduced. Every time, before choosing a new bias, we have put the system in feedback such that the tip can change the distance accordingly upon increasing the bias, to keep the current chosen by the set-point.

In figure 4.1 we present the spectra of our measurements. The PT peaks and its multiples are clearly visible. But it is difficult to compare the measurements, and with that to see whether the peaks are dependent on the bias (i.e. tip sample distance) or having the system in feedback or not. To investigate this we zoom into the multiples. We present the main peak (1.4 Hz) and the first two multiple (2.8 & 4.2 Hz) in figure 4.2. What becomes apparent is that the PT peaks are all equally high, independent of the bias voltage V_b, or having the system in feedback or not.

We want to investigate this quantitatively as well. To do this, we integrate the power densities around the PT multiples. We found that the PT peaks are apparent in the spectra until the 21th multiple of 1.4 Hz, that means until around 29.4Hz. Therefore, to make calculations more manageable, we only added the contributions of the PT until the 21th multiple. Also, we noticed that the 21th multiple of the PT occurs at 29.36 Hz, which implies that:

$$\text{The pulse tube pumps at } 29.36/21 \sim 1.398 \text{ Hz}$$

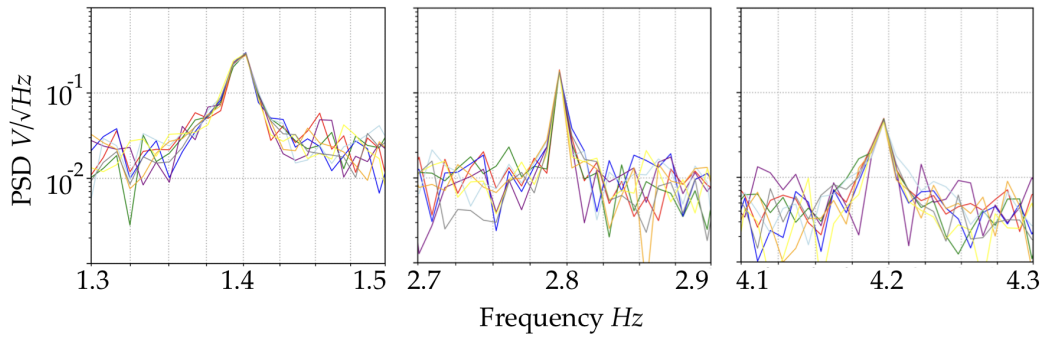

Figure 4.2: *First three pulse tube peaks (1.4 Hz, 2.8 Hz and 4.2 Hz). The contribution of the PT to the noise spectrum is independent of the bias voltage and thus the tip-sample distance.*

For every multiple of the PT we integrate the power within 0.2 Hz around the multiple (as plotted in fig. 4.2). We estimated by eye that this would be a region that ensures us that we add the entirety of a peak, without adding too much of the surrounding background noise. The peaks of the multiples are generally orders of magnitude higher than the background noise, therefore, we expect the contribution of the actual peak to be leading over the background noise. And thus, having a possibly too wide range is not too big of an issue. Doing these calculations yield the values presented in table 4.1. The different measurements have surprisingly equal contribution from the PT. On average the contribution of the PT until the 21th multiple is $\langle \sigma^2 \rangle \sim 0.000872 V^2$. Taking the square-root we obtain root-mean-square value. Where in the last equality we use the fact that the I/V-converter has a gain of 10^9.

$$V_{RMS} = \sigma \sim 30\,\mathrm{mV}_{RMS} = 30\,\mathrm{pA}_{RMS}$$

Now, to the feedback system it does not matter where the noise enters the system. If the feedback works properly it will respond and actuate the scan tube to counter the $30\,\mathrm{pA}_{RMS}$ oscillation at 1.4 Hz. At a set-point of 100 pA this is achieved if the tip oscillates with an RMS amplitude of $\sim$ 0.18 Å. Because, assuming a linear regime, the current would counter oscillate between RMS values 70 pA and 130 pA. Then, through equation 2.5, we know this corresponds to a - 0.18 Å to + 0.13 Å oscillation around z_0 in figure 2.4.

The pulse tube will cause the tip to vibrate
with an RMS amplitude of $\sim$ 0.18Å

Measurement	σ^2 [V^2_{RMS}]	σ [mV_{RMS}]
$V_b = 0.5$ & feedback	0.000905	30.1
$V_b = 0.5$ & frozen	0.000846	29.1
$V_b = 1.0$ & feedback	0.000897	29.9
$V_b = 1.0$ & frozen	0.000862	29.9
$V_b = 1.5$ & feedback	0.000844	29.4
$V_b = 1.5$ & frozen	0.000845	29.0
$V_b = 2.0$ & feedback	0.000905	29.1
$V_b = 2.0$ & frozen	0.000873	30.1

Table 4.1: *Power contribution of the noise caused by the PT.*

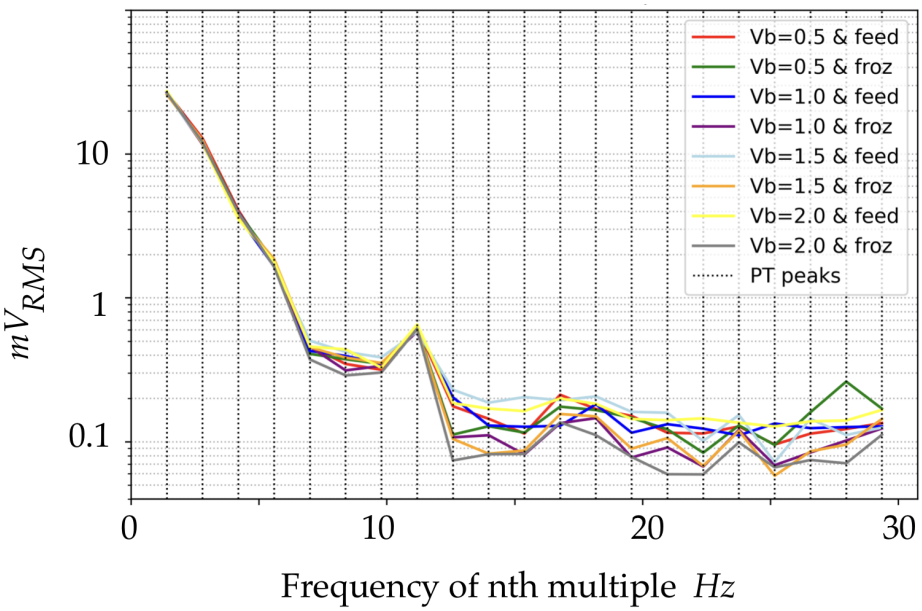

Figure 4.3: *Contribution of the PT multiples until the 21th multiple. We observe that the contribution of the PT is the same for all the measurements that were done, with different biases and with feedback on/off. Note: the continuous line is used to easily separate the measurements, but misleading as the contributions only hold AT the multiples.*

Version of March 7, 2024– Created March 7, 2024 - 11:58

Conclusion and discussion

Our results propose that the pulse tube contributes 30 pA_{RMS} of vibrations to the tip-current, with properly functioning feedback, this results in a vibration of the tip of $\sim$ 0.18Å. We suggest that this does not prevent us from achieving step-edge resolution, but do not know yet if this prevents us from achieving atomic resolution. Furthermore, we propose that the dominant contribution of PT vibrations enters due to microphonics around the I/V-converter and its cables, explain why we think we can reduce this effect and give an advice on how to do so.

We suggest two dominant sources through which the vibrations may enter the system. First of all, the pulse tube could cause the tip-sample distance to change, in turn changing the tip-current through eq. 2.1. Secondly, the pulse tube could cause vibrations of the I/V-converter and its cables which due to microphonics enter as currents. Figures 4.2 and 4.3 show that the PT peaks are independent on the bias and with that the tip-sample distance. Which leads us to the conclusion that the main contribution from the PT is not due to an oscillation in sample tip distance and we hypothesise that currently the vibrations are due to microphonics of the I/V-converter and its cables. If the main contributor would be the vibration of the tip or the sample, we would expect that increasing or decreasing the tip-sample distance would result in less or more transmission of the vibration, respectively. Because, for every 1Å increase in tip-sample distance, the current increases roughly 10 times. We do not observe this. Additionally, while doing various measurements and playing around with the setup, we noticed that the I/V-converter is very sensitive to vibrations. When we touched it lightly by hand, we would immediately notice this in the current. We suggest to try to reduce the effect of microphonics around the I/V-converter. After the tip-current goes through the I/V-converter it becomes a voltage signal, which is less prone to microphonics than a current signal. Therefore, we assume the microphonics enter before the I/V-converter, around the point where we connect to the cryostat wiring to the 2-point mini LEMO cable and the connection with the I/V-converter.

Initially the I/V-converter was fixed on the inner frame, which vibrates at 1.4Hz, with a layer of foam in between, in the hopes that this would lessen the PT vibrations. By hanging the I/V-converter in springs we might reduce these PT vibrations. However, these springs can still transmit vibrations at its own resonance frequency. Another suggestion would be to mount the I/V-converter onto the cryostat and to fix the coax wire firmly to the frame. This way we ensure that, although vibrating, all com-

ponents vibrate equally, reducing relative vibrations, and with that microphonics.

Furthermore, in figures 4.2 and 4.3 we observe that the observed spectra did not depend on turning feedback on or off. This leads us to the conclusion that the feedback system was not working properly. Good functioning feedback should be able to reduce the effect of a 1.4Hz vibration. We have not resolved the cause of this result. We think it might have to do with a very large integration time which is not able to respond to 1.4Hz vibrations. However, when choosing different set-points, we observed that the tip-current reached the new set-point within roughly half a second. First of all, indicating that the scan tube is working. And secondly, suggesting that the integration time was not too long. We suggest to do this experiment again, with these considerations in mind, and to also record the the voltage that is sent to the Z-piezo.

Finally, we want to put the contribution of the pulse tube into perspective. We measured that the PT contributes a 30 pA_{RMS}, which through the feedback system we expect to cause a vibration of the tip with an RMS amplitude of $\sim$ 0.18Å. We know that the distance between two layers of HOPG is about 3.35 Å [6] and the distance between nearest neighbours in an HOPG sample is about 2.46 Å [16]. Thus, the vibrations caused by the PT cause vibrations to the tip that are more then a tenfold smaller than the features we are trying to distinguish for step-edge resolution. Therefore, at this point, we suggest that the contribution of the pulse tube will not prevent us from achieving step-edge resolution. To determine whether it could prevent us from achieving atomic resolution we would need to quantify the change in current caused by individual atoms. For this we suggest a better literature research or to simulate the measured current caused by neighbouring atoms as described in sec. 2.2. Having said that, Den Haan et al. (2014) [12] achieved atomic resolution in the *Oosterkamp group* and presented their measured spectra as well (figs. 2.6 & 4.4). Their pulse tube contribution was of the order of 1pA_{RMS} (adding the 1.4 Hz multiples). Which is 30 times lower then what we measured for our set-up. The 30 times better result makes it reasonable to assume that we are currently doing something sub-optimal and so we want to try to reduce the effect of microphonics.

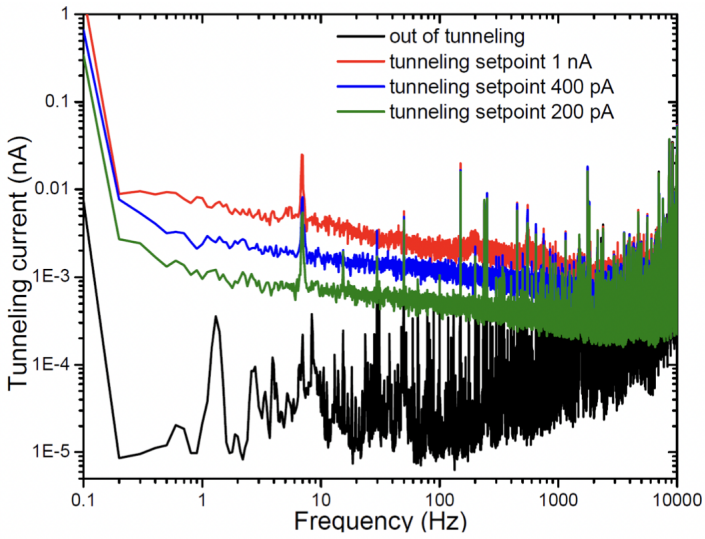

Figure 4.4: *Figure and caption from A. den Haan et al. 2014 [12]: "Tunnel-spectrum for several tunneling current set-points. Most of the noise (peaks) visible in the out of tunneling spectrum are due to microphonics"*

4.2 Ultra cold spectra analysis Out of tunneling vs. in tunneling

In the previous section we reasoned that the 30 pA_{RMS} noise, caused by the PT, is not due to a vibrating tip or sample. In this section we present another route to validate this claim. If the current PT contribution is not caused by the changing tip-sample distance, we must have an equal contribution when out of tunneling range. In this section we present spectra of tip-current measurements out of tunneling range, which show a PT contribution of 30 pA_{RMS}. Equal to the PT contribution of tip-current measurements in tunneling range (sec. 4.1). Further supporting the conclusion that, at this point, the dominating vibrations are entering around the I/V-converter and the cables due to microphonics.

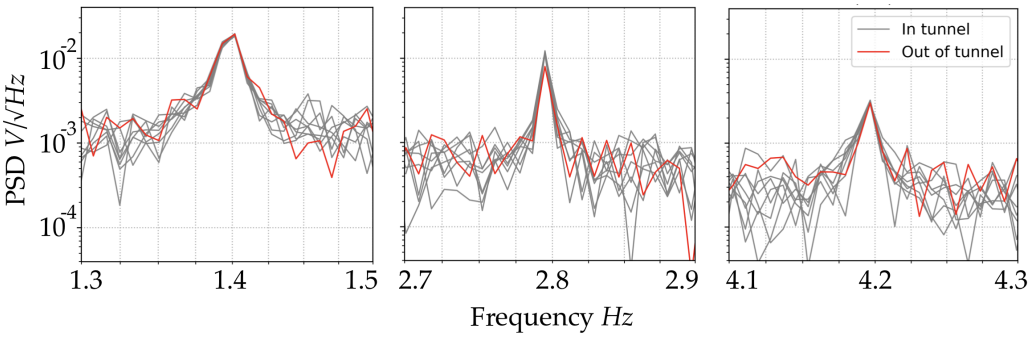

Figure 4.5: *First three pulse tube peaks (1.4 Hz, 2.8 Hz and 4.2 Hz). The contribution of the PT to the noise spectrum is the same for a tip-current out of tunneling range and in tunneling range.*

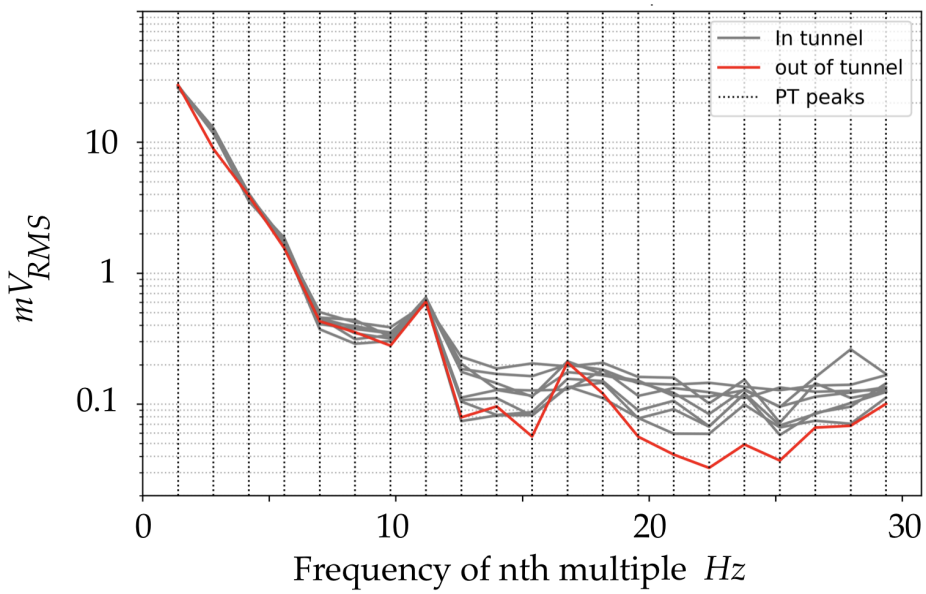

Figure 4.6: *Contribution of the PT multiples until the 21th multiple. Out of tunnel PT contributions follow the in tunnel measurements well up to the 14 multiple. Note: the continuous line is used to easily separate the measurements, but misleading as the contributions only hold AT the multiples.*

4.3 Room temperature spectra analysis Changing set-up to reduce microphonics

Now that we hypothesized that the 30 pA_{RMS} noise caused by the PT is due to microphonics around the I/V-converter, we want to try to improve the setup. In this section we present our solution and how it resulted in reduction of microphonics. Initially, the I/V-converter was mounted onto the inner frame, with a piece of foam in between, because we thought this would add vibration isolation. Now, we think that this setup is disadvantageous and causes the connection between the cable and the cryostat to vibrate differently from the connection between the cable and the I/V-converter (red cable with blue tape in fig. 4.7). This relative motion would then be the source of the microphonics. In order to reduce this relative motion we mounted the I/V-converter directly to the cryostat as shown in fig. 4.7 and fixed the wire firmly to the frame. This way we ensure, although vibrating, all components vibrate equally, reducing relative vibrations, and with that microphonics.

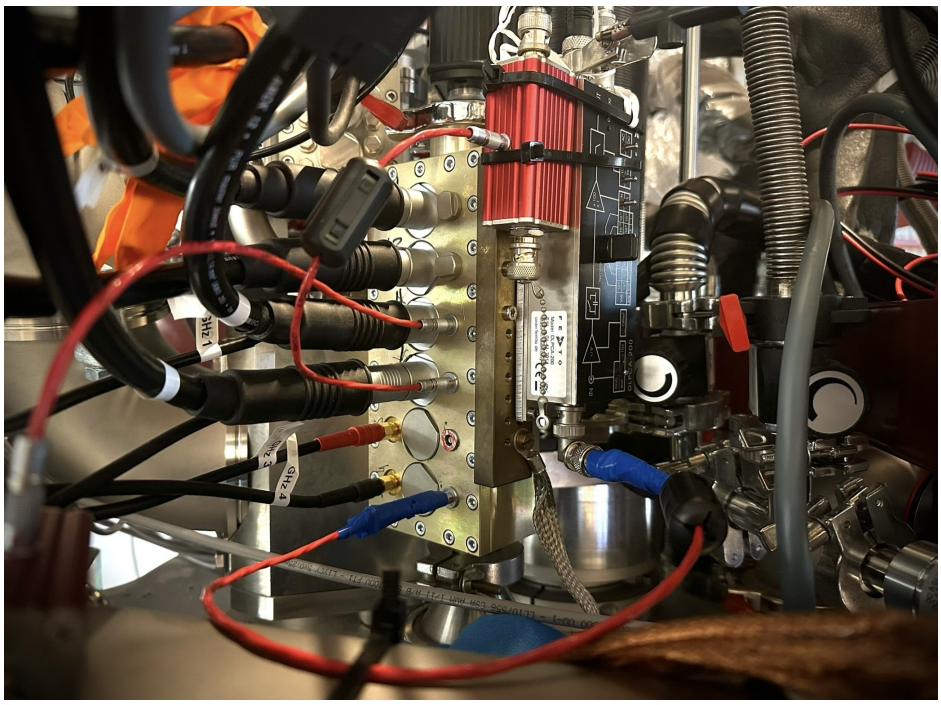

Figure 4.7: *Picture of how we mounted the I/V-converter to the cryostat to reduce microphonics of the cables.*

Result

At room-temperature we measured the tunneling current with feedback on and off. In fig. 4.8 we present the spectra. We clearly observe that having the system in feedback reduces the noise. Furthermore, the pulse tube peaks are not visible anymore as they are drowned by the noise floor. We can follow the exact same procedure as described in sec. 4.1 to determine the contribution to the noise around the pulse tube peaks by integrating the power densities 0.2 Hz around the peaks, up until the 21th multiple. Even though the pulse tube peaks are now drowned by the noise floor, the value serves as an upper-bound. Doing this calculation yields that the upper bound to the noise contribution of the pulse tube is:

$$V_{RMS} = 4\ \text{mV}_{RMS} = 4\ \text{pA}_{RMS}$$

Furthermore, using eq. 2.5, and the 100 pA set-point, we can relate this noise to a vibration of the tip. Doing this calculation yields that the upper-bound of the pulse tube vibrations would cause the tip to vibrate with an RMS amplitude of ~ 0.02Å.

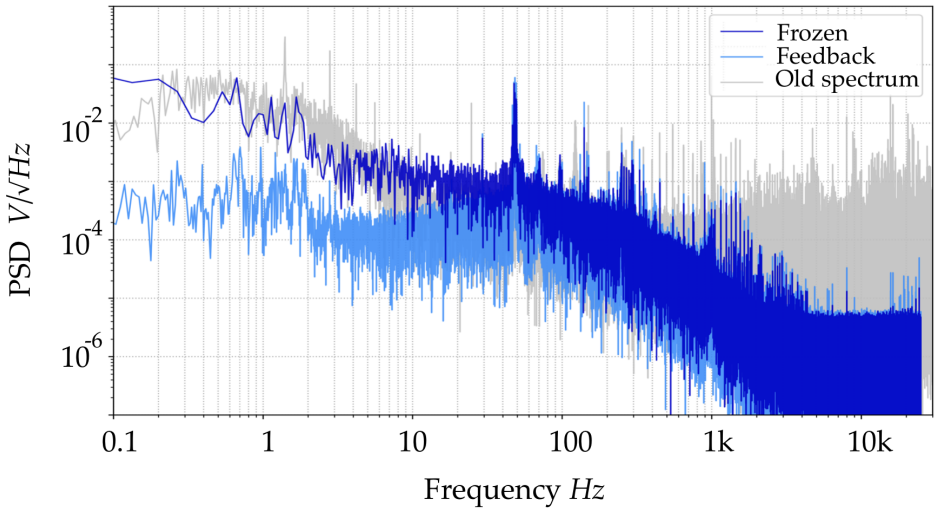

Figure 4.8: *Spectra of the tunnel-current at 100 pA set-point, with I/V-converter mounted to the cryostat. With feedback frozen we only observe the 1.4 Hz peak. Furthermore, we get a significant noise contribution at low frequencies. Different from our first measurements in sec. 4.1, we now observe significantly less noise when having the system in feedback. Also, in feedback the PT peaks are not visible anymore.*

Version of March 7, 2024– Created March 7, 2024 - 11:58

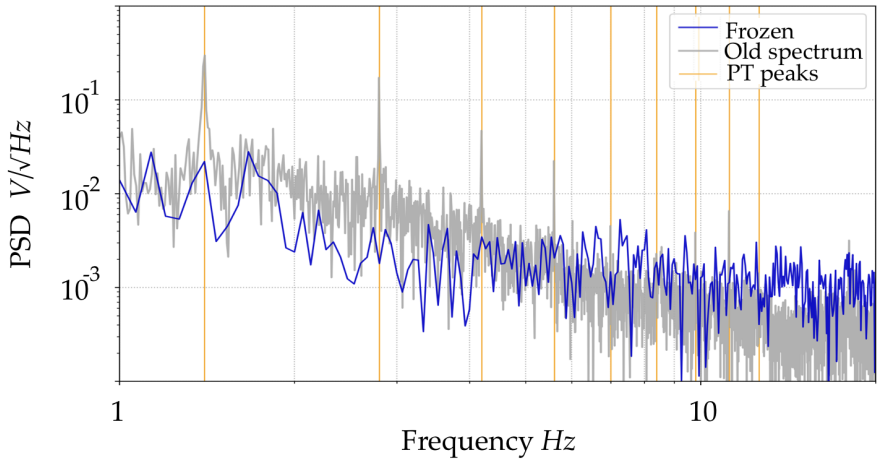

Figure 4.9: *Spectra of fig. 4.8, zoomed-in to visualise the pulse tube peaks. Notice that all the pulse tube peaks, that are prominently visible in the spectra from sec. 4.1 (old spectrum), are not visible anymore and drowned by the noise floor.*

Conclusion and discussion

After improving the set-up to reduce the effect of microphonics the pulse tube peaks are no longer visible anymore, as they are drowned by the noise floor. This means that the upper-bound of the noise contribution from the pulse tube at 100 pA set-point is 4 pA_{RMS}, 4% of the set-point, which through the feedback system would lead to $\sim$ 0.02Å. This value is within the range of $0.0002 - 0.2$Å that we expect the mechanical vibration to cause if we model the STM as a mass-spring system (sec. 3.3). This should not prevent us from achieving step-edge resolution and we are very hopeful that it should also not prevent us from achieving atomic resolution, as the oscillation is more than hundred times smaller than the distance between HOPG layers (3.35 Å [6]) or the distance between neighbouring carbon atoms (2.46 Å [16]). Our upper-bound to the pulse tube contribution is now only 4 times larger than the actual contribution measured by den Haan et al. [12]. Which is promising as we still see potential to improve on our result.

Namely, we discovered that doing measurements with feedback frozen is very hard due to piezo creep. In fig. 4.10 we plot the current of which we calculated the Fourier transform to produce the spectra from figs. 4.8 and 4.9. Taking the Fourier transform of the entire measurement leads to a drastically raised noise floor and a 34 pA_{RMS} pulse tube peak at 1.4 Hz. However, this is misleading as the current did not stay at 100 pA, rather it increased to 10 nA. At 1 nA, 4% leads to 40 pA_{RMS}. At 10 nA, 4% leads to

400 pA_{RMS} noise. But the noise only makes sense when we can relate it to a certain set-point. Therefore, for the Fourier transform we only used the first 15 seconds, where the current was relatively constant around 10-300 pA. Still this range is large and can be improved, but it already leads to an upper-bound of 4 pA_{RMS} at 100 pA set-point. To improve on this result we suggest to repeat this measurement, but to wait until the piezo creep has finished before starting the measurement. By monitoring capacitive read-out of the lock-in amplifier, which we can use as a measure for the tip-sample distance, we observed that the piezo creep slowly stagnates but that it takes more than an hour to reach a relatively constant situation, at room-temperature. Also, we would like to do the measurement at ultra-low temperatures. To investigate if that makes a difference. But the piezo-creep will be even slower at these temperatures. To keep track of the piezo-creep we suggest monitoring the capacitive read-out of the lock-in amplifier.

Lastly, in fig. 4.8 we observe that having the system in feedback reduces the noise significantly as we would expect properly functioning feedback to do. We have not found the reason as to why we did not observe this distinction in our measurements of sec. 4.1. To confirm whether feedback is working properly we also investigated the spectra of the feeedback signal that is sent to the Z-piezo, both in feedback and with feedback frozen. Results are shown in fig. 4.11. As we would expect from properly functioning feedback, the spectrum in feedback lies much higher than with feedback frozen. Also, pulse tube peaks are visible in the spectrum of the feedback signal, meaning that the feedback system is correctly responding to the pulse tube vibrations in the current.

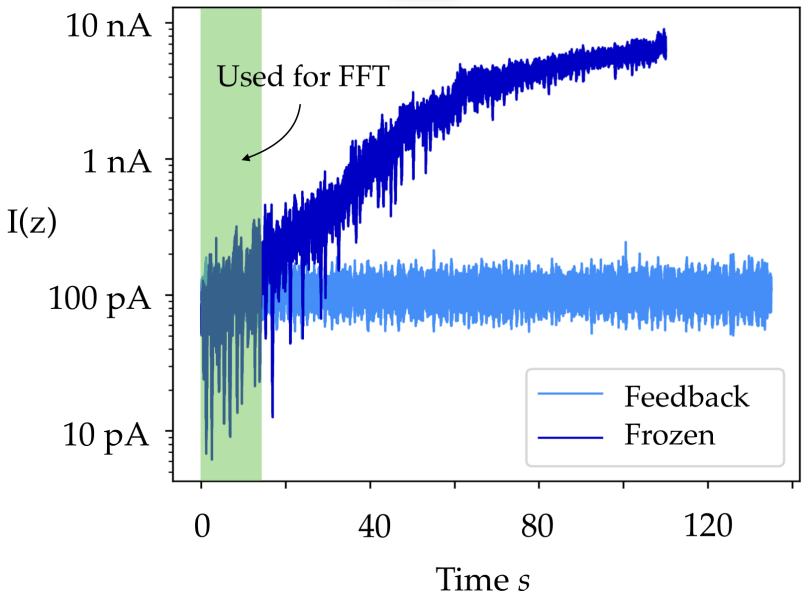

Figure 4.10: *Tunnel-current measurements that we used to produce the spectra from figs. 4.8 and 4.9. The current with feedback frozen is increasing due to piezo creep. Therefore, for the frozen measurement, we only used the first 15 seconds (green) to calculate the FFT.*

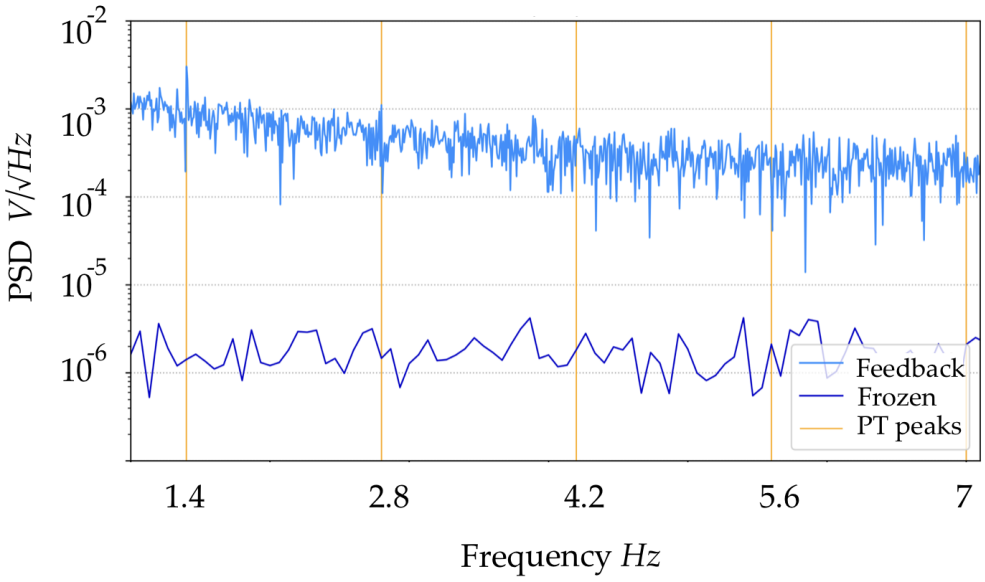

Figure 4.11: *Spectra of the feedback signal that is sent to the Z-piezo of the scan tube. The feedback signal lies significantly higher than with feedback frozen and shows peaks around the PT multiples.*

4.4 Scanning

In this section we present our scanning result with the *Basic-STM* and *Nanonis*, at room temperature and at ultra-low temperature.

Room-temperature

At room temperature we achieved a scan with clearly visible step-edges and an improved resolution compared to the scan we achieved a couple of months ago which is shown in fig. 2.6. The scan in fig. 2.6 was produced with a setup containing a different STM, digital program (*Camera*), tip and sample. It is not clear what caused this improved resolution. But, the different program *Nanonis* allowed for better tuning during test scans and searching for good scan locations, which helped us while scanning.

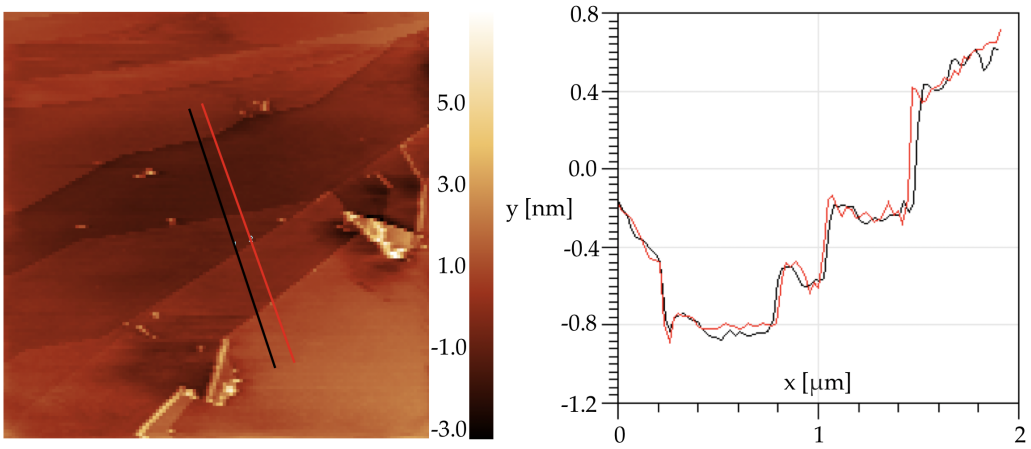

Figure 4.12: *Room temperature scan with the Basic-STM done in constant current mode. 3μm $\times$3μm. The step-edges are visible and the resolution has significantly improved. Right: line-plot of the 1D lines on the scan. When step edges are clearly visible we can use the line plot to calibrate our setup, as a step-edge should be a multiple of 3.35 Å (sec. 3.1).*

Ultra-low temperature

At ultra-low temperatures we were not able to produce scans with such clear features as fig. 4.12. It is not clear what caused this, but it is clear that scanning at ultra-cold temperatures is more challenging. Also, initially the motors were not able to move at ultra-low temperatures, so significant

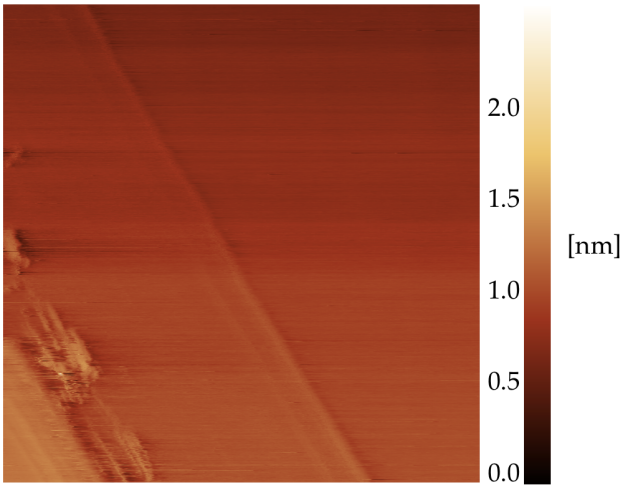

Figure 4.13: *300 nm × 300 nm scan at ultra-low temperatures with a double-tip, causing features to appear double.*

time was spent on optimizing the parameters as explained in sec. 3.2. Another factor that makes scanning at these temperatures more challenging, is the 4-5 times reduced range of the scan tube, as we are at maximum scanning a surface 4-5 times smaller than fig. 4.12, making it less likely to come across a step edge, which is the first visible feature, so without it is very hard to fine tune the STM. Fortunately, we also have a coarse X-motor, so we can approach at multiple spots on the sample, and search for a step edge. After extensive search we were able to observe what seems to be a step-edge. We also found out that we were scanning with a double-tip (sec. 2.1), as the features appear twice.

Chapter 5

General Conclusion and Outlook

One of the aims of this research was to investigate and quantify the noise on the tip-current caused by the vibrations of the pulse tube. We found that the dominant contribution entered through microphonics around the I/V-converter and the cables that are connected to it, rather than a changing tip-sample distance. This gave rise to 30 pA_{RMS} noise with clear pulse tube peaks. By mounting the I/V-converter directly to the cryostat and fixing the 2-point mini LEMO cable firmly to the inner frame we successfully reduced the effect of microphonics. The pulse tube peaks are no longer visible and drowned by the noise floor. Integrating the power spectral density around the pulse tube peaks gives an upper-bound to the pulse tube vibrations of 4 pA_{RMS}, which corresponds to 4% of the set-point.

With a properly operating feedback system, the 4 pA_{RMS} noise will cause the scan tube to counter oscillate at 1.4 Hz with an RMS amplitude of $\sim$ 0.02Å, which is within the range of $0.0002 - 0.2$Å that we expect the mechanical vibration to cause if we model the STM as a mass-spring system (sec. 3.3). Furthermore, this vibration is more than hundred times smaller than the distance between HOPG layers (3.35 Å [6]) or the distance between neighbouring carbon atoms (2.46 Å [16]). Therefore, we believe that the oscillations of the pulse tube will not prevent us from achieving step-edge resolution. And are very hopeful that it will also not prevent us from achieving atomic resolution. Thus, at this point, we do not see the need for another mass-spring system specifically for the STM. Having said that, den Haan et al. (2014) [12] achieved atomic resolution with a pulse tube contributions around 1 pA_{RMS}, only 4 times larger than our upper-bound, that we even see potential for to improve on by doing new measurements of the feedback frozen current, this time at ultra-low temperatures and by first letting the piezo creep stagnate. To monitor this

one can keep track of the capacitive read-out of the STM-junction on the lock-in amplifier.

Furthermore, we were able to produce new scanning results at room-temperature (fig. 4.12) that show a significant improvement in resolution compared to the starting point of this project (fig. 2.6). We clearly observe the step-edges and the line-plot shows sharp distinctions between the size of step-edges. Also, we were able to observe features at ultra-low temperatures for the first time since 2014. We devote part of this improvement to a better digital analysis system called *Nanonis* and believe that purchasing this operating system will help the *Oosterkamp Group* doing quality measurements in the future. Now that we have drastically reduced the effect of microphonics it is very exciting to do new scanning and spectroscopy measurements ones *Marshmallow* is cooled down again.

Chapter 6

Acknowledgement

I would like to devote a couple of words to the people that have helped me throughout this amazing journey at the Oosterkamp group. I could not have imagined how great of a learning experience these months would be for me.

When I started the project, Tjerk, Koen and I discussed what would be the aim for my research. I thought it would take a couple of weeks of work and then we would have to look for a new goal. I underestimated Scanning Tunneling Microscopy, experimental physics, the patience one needs for it, and the ability one needs to deal with set-backs. Every time we solved one problem, something else broke. While I was still sad about something had broken, Koen was already enthusiastically thinking about the solution. I remember the first weeks really thinking: "How does he do it?". But quickly I started to enjoy it and be very grateful for it. Because every set-back was a new puzzle that required me to think on my own and helped me to understand better what it takes to be an experimentalist.

Koen, I enjoyed greatly working with you every day. I am very grateful for your mentoring and you really helped me so that I could learn the most these months. From the day that I started I felt taken seriously by you, because whenever I made a suggestion you immediately said "That's a good idea, let's try it". Your experimental qualities were also fascinating to me and I hope that you will manage to produce a scan with atomic resolution inside the cryostat.

Tjerk, I want to thank you for giving me this incredible learning experience at your lab. It is inspiring to see how you were always able to translate my work in the lab to general learning insights of being an experimentalist. And I hope that I will be able to do this as well in the future.

Also, I want to thank Prof. van Ruitenbeek for being my second su-

pervisor and for thinking with me about the orientation with respect to gravity of the course-motors when we were having trouble with getting them to walk.

Thanks also to David to always be there to help Koen and I resolve issues with the STM. And thanks to the people from ELD and FMD who were there to help us build the components we needed.

Lastly, I want to thank the other members from the Oosterkamp group, Jaimy, Dennis, Lars and Loek, and the members from the Hensen group, for having a fun time throughout.

Bibliography

[1] Esta Abelev, Nina Sezin, and Yair Ein-Eli. "An alternative isolation of tungsten tips for a scanning tunneling microscope". In: *Review of Scientific Instruments - REV SCI INSTR* 76 (Oct. 2005). DOI: 10.1063/1.2075187.

[2] F. Atamny, O. Spillecke, and R. SchlÃ¶gl. "On the STM imaging contrast of graphite: towards a âtrueâ' atomic resolution". In: *Phys. Chem. Chem. Phys.* 1 (17 1999), pp. 4113–4118. DOI: 10.1039/A904657G. URL: http://dx.doi.org/10.1039/A904657G.

[3] G. Binnig et al. "Surface Studies by Scanning Tunneling Microscopy". In: *Phys. Rev. Lett.* 49 (1 July 1982), pp. 57–61. DOI: 10.1103/PhysRevLett.49.57. URL: https://link.aps.org/doi/10.1103/PhysRevLett.49.57.

[4] K. Bisina and Maleeha Abdul Azeez. "Optimized estimation of power spectral density". In: (June 2017), pp. 871–875. DOI: 10.1109/ICCONS.2017.8250588.

[5] Li Bowen et al. "Fabricating ultraâsharp tungsten STM tips with high yield: doubleâelectrolyte etching method and machine learning". In: *SN Applied Sciences* (2020), pp. 2523–3971. DOI: 10.1007/s42452-020-3017-4. URL: https://doi.org/10.1007/s42452-020-3017-4.

[6] Hsiangpin Changf and Allen J. Bard. "Observation and Characterization by Scanning Tunneling Microscopy of Structures Generated by Cleaving Highly Oriented Pyrolytic Graphite". In: *Journal of Vaccuum Science and Technology A* Department of Chemistry, The University of Texas at Austin, Austin, Texas 78712 (1990). DOI: 10.1021/la00054a021. URL: http://pubs.acs.org.

[7] C. Julien Chen. “Introduction to Scanning Tunneling Microscopy - Third Edition”. In: *MONOGRAPHS ON THE PHYSICS AND CHEMISTRY OF MATERIALS - 69 - Oxford Science Publications - Department of Applied Physics and Applied Mathematics, Columbia University, New York* (2021), pp. 2, 4, 367.

[8] P. Das, R.B. Ouboter, and K.W. Taconis. “A Realization of a London-Clarke-Mendoza Type Refrigerator”. In: *Low Temperature Physics LT9, Springer, Boston, MA* (1965), pp. 1253–1255. DOI: 10.1007/978-1-4899-6443-4_133. URL: https://link.springer.com/chapter/10.1007/978-1-4899-6443-4_133.

[9] Femto - Lase Components - Datasheet. “Current/Transimpedance Amplifiers - Ultra-Low-Noise-Amplifiers For High-Speed precision Measurements”. In: (), Page 2 - 12/19/ V03 / KK-HW / femto/ overview–amplifier. URL: https://www.lasercomponents.com/de/?embedded=1&file=fileadmin/user_upload/home/Datasheets/femto/overview-amplifiers.pdf&no_cache=1.

[10] Francis Duck. “The Electrical Expansion of Quartzâ by Jacques and Pierre Curie. Ultrasound”. In: (2009), 17(4):197–203. DOI: 10.1179/174227109X12500830049951.

[11] R.M. Feenstra, Joseph A. Stroscio, and A.P. Fein. “Tunneling spectroscopy of the Si(111)2 Ã 1 surface”. In: *Surface Science* 181.1 (1987), pp. 295–306. ISSN: 0039-6028. DOI: https://doi.org/10.1016/0039-6028(87)90170-1. URL: https://www.sciencedirect.com/science/article/pii/0039602887901701.

[12] A.M.J. den Haan et al. *Atomic resolution STM in a cryogen free dilution refrigerator at 15 mK*. Vol. 85. Review Of Scientific Instruments, 2014, p. 035112. DOI: https://doi.org/10.1063/1.4868684. URL: https://doi.org/10.1063/1.4868684.

[13] Jr.; S. L. Brandow; R. A. Brizzolara; N. A. Burnham; D. P. DiLella; K. P. Lee; C. R. K. Marrian; R. J. Colton J. P. Ibe; P. P. Bey. “On the electrochemical etching of tips for scanning tunneling microscopy”. In: *Journal of Vaccuum Science and Technology A* J. Vac. Sci. Technol. A 8, 3570â3575 (1990). URL: https://doi.org/10.1116/1.576509.

[14] Jim Karki. “Active Low-Pass Filter Design”. In: *Texas Instruments - AAP Precision Analog* (2023), p. 1.

[15] Kensuke Kobayashi and Masayuki Hashisaka. “Shot Noise in Mesoscopic Systems: From Single Particles to Quantum Liquids”. In: *Journal of the Physical Society of Japan* 90.10 (Oct. 2021), p. 102001. ISSN: 1347-4073. DOI: 10.7566/jpsj.90.102001. URL: http://dx.doi.org/10.7566/JPSJ.90.102001.

[16] M. Kuwabara, D. R. Clarke, and D. A. Smith. “Anomalous superperiodicity in scanning tunneling microscope images of graphite”. In: *Applied Physics Letters* 56.24 (June 1990), pp. 2396–2398. ISSN: 0003-6951. DOI: 10.1063/1.102906. eprint: https://pubs.aip.org/aip/apl/article-pdf/56/24/2396/7502127/2396_1_online.pdf. URL: https://doi.org/10.1063/1.102906.

[17] Jiutao Li, Wolf-Dieter Schneider, and Richard Berndt. “Local density of states from spectroscopic scanning-tunneling-microscope images: Ag(111)”. In: *Phys. Rev. B* 56 (12 Sept. 1997), pp. 7656–7659. DOI: 10.1103/PhysRevB.56.7656. URL: https://link.aps.org/doi/10.1103/PhysRevB.56.7656.

[18] Quanfeng Li and Qingyou Lu. “Atomic resolution ultrafast scanning tunneling microscope with scan rate breaking the resonant frequency of a quartz tuning fork resonator”. In: *The Review of scientific instruments* 82 (May 2011), p. 053705. DOI: 10.1063/1.3585200.

[19] Yingzi Li et al. “A double-electrolyte etching method of high-quality tungsten probe for undergraduate scanning tunneling microscopy and atomic force microscopy experiments”. In: *European Journal of Physics* 40 (Dec. 2018). DOI: 10.1088/1361-6404/aaf5e4.

[20] Gabor Mandi, Gilberto Teobaldi, and Krisztian Palotas. “Contrast stability and âstripeâ formation in scanning tunnelling microscopy imaging of highly oriented pyrolytic graphite: the role of STM-tip orientations”. In: *Journal of Physics: Condensed Matter* 26.48 (Oct. 2014), p. 485007. ISSN: 1361-648X. DOI: 10.1088/0953-8984/26/48/485007. URL: http://dx.doi.org/10.1088/0953-8984/26/48/485007.

[21] Eugen Merzbacher. “The Early History of Quantum Tunneling”. In: *Physics Today* 55.8 (Aug. 2002), pp. 44–49. ISSN: 0031-9228. DOI: 10.1063/1.1510281. eprint: https://pubs.aip.org/physicstoday/article-

pdf/55/8/44/8316712/44_1_online.pdf. URL: https://doi.org/10.1063/1.1510281.

[22] V. L. Mironov. "The textbook for students of the senior courses of higher educational institutions". In: *Fundamentals of Scanning Probe Microscopy - Nizhniy Novgorod* (2004).

[23] Sumati Patil, Sadhu Kolekar, and Aparna Deshpande. "Revisiting HOPG superlattices: Structure and conductance properties". In: *Surface Science* 658 (2017), pp. 55–60. ISSN: 0039-6028. DOI: https://doi.org/10.1016/j.susc.2016.12.002. URL: https://www.sciencedirect.com/science/article/pii/S0039602816306525.

[24] Kachoosangi Roohollah Torabi and Compton Richard G. "A simple electroanalytical methodology for the simultaneous determination of dopamine, serotonin and ascorbic acid using an unmodified edge plane pyrolytic graphite electrode". In: *Springer-Verlag - Analytical and Bioanalytical Chemistry* 387 (2006), pp. 2793–2800. DOI: 10.1007/s00216-007-1129-y.

[25] Michael Schmid and Grzegorz Pietrzak. "Schematic diagram of a scanning tunneling microscope". In: *TU Wien; adapted from the IAP/TU Wien STM Gallery* (May 2020). URL: https://en.wikipedia.org/wiki/Scanning_tunneling_microscope#/media/File:Scanning_Tunneling_Microscope_schematic.svg.

[26] Onnes Technologies. *Cryo-walking technology*. 2023. URL: https://onnestechnologies.com/technology/.

[27] Onnes Technologies. *Cryo-walking technology - product description*. 2023. URL: https://onnestechnologies.com/products/arqtika/.

[28] J. Tersoff and D. R. Hamann. "Theory of the scanning tunneling microscope". In: *Phys. Rev. B* 31 (2 Jan. 1985), pp. 805–813. DOI: 10.1103/PhysRevB.31.805. URL: https://link.aps.org/doi/10.1103/PhysRevB.31.805.

[29] Michael Y. Toriyama et al. "How to analyse a density of states". In: *Materials Today Electronics* 1 (2022), p. 100002. ISSN: 2772-9494. DOI: https://doi.org/10.1016/j.mtelec.2022.100002. URL: https://www.sciencedirect.com/science/article/pii/S277294942200002X.

[30] Frank Trixler. "Quantum Tunnelling to the Origin and Evolution of Life". In: *Current organic chemistry* 17 (Aug. 2013), pp. 1758–1770. DOI: 10.2174/13852728113179990083.

[31] J.M. de Voogd et al. *Fast and reliable methods for determining the evolution of uncertain parameters in differential equations*. Vol. 2. 2023, pp. 530–556. DOI: https://doi.org/10.1016/j.jcp.2005.08.024. URL: https://www.sciencedirect.com/science/article/pii/S0021999105003918.

[32] Jelmer J.T. Wagenaar. "Physics Experiments 2 - Signal Processing and Noise". In: (2020).

[33] Shuai Zhang, Di Huang, and Shiwei Wu. "A cryogen-free low temperature scanning tunneling microscope capable of inelastic electron tunneling spectroscopy". In: *Review of Scientific Instruments* 87.6 (June 2016), p. 063701. ISSN: 0034-6748. DOI: 10.1063/1.4952577. eprint: https://pubs.aip.org/aip/rsi/article-pdf/doi/10.1063/1.4952577/15887185/063701_1_online.pdf. URL: https://doi.org/10.1063/1.4952577.